Quantum Confinement Effects on the Energy Gaps of PbSe Semiconductor Thin Films Created Using Electrochemical Atomic Layer Epitaxy

by

Stephen Matthew Cox

(Under the direction of Uwe Happek)

Abstract

Thin film PbSe semiconductors created using the method of electrochemical atomic layer epitaxy (EC-ALE) were found to exhibit changes in the fundamental energy gap with respect to film thickness. Quantum confinement of the electron-hole pair due to thickness restrictions imposed on PbSe thin films is presumed to be the primary cause of the energy gap changes, which are compared to both parabolic and hyperbolic band theory models of quantum confinement. Transmittance spectra of the thin films were determined from Fourier transform infrared spectroscopy (FTIR), and energy gaps were determined from the analysis of subtle features of the measured absorption coefficient. Atomic force microscopy was employed to study the surface character of the semiconductor thin films, and their future study is recommended to involve methods of electron beam lithography and scanning tunneling spectroscopy.

Index words: Electrochemical atomic layer epitaxy, EC-ALE, Compound semiconductor, Quantum confinement, Thin film, PbSe, Electron beam lithography

Quantum Confinement Effects on the Energy Gaps of PbSe Semiconductor Thin Films Created Using Electrochemical Atomic Layer Epitaxy

by

Stephen Matthew Cox

B.S., The University of Georgia, 2001

A Thesis Submitted to the Graduate Faculty
of The University of Georgia in Partial Fulfillment
of the
Requirements for the Degree

Master of Science

Athens, Georgia

2003

Quantum Confinement Effects on the Energy Gaps of PbSe Semiconductor Thin Films Created Using Electrochemical Atomic Layer Epitaxy

by

Stephen Matthew Cox

Approved:

Major Professor: Uwe Happek

Committee: John Stickney
William Dennis

Electronic Version Approved:

Maureen Grasso
Dean of the Graduate School
The University of Georgia
August 2003

Acknowledgments

I would like to thank my family for encouraging me to continue my education in pursuit of this degree. My mother Nancy and my father William have been unflinchingly supportive and patient throughout all of my academic pursuits and frivolous detours. I'll graduate someday, I promise. Also, I am graciously indebted to my sister, Susan, and my brothers, Greg and Mike, for giving me a place to stay and pats on the back. I'd do anything for you all. I also found great comfort from conversations with my uncle, Richard, about the pressures involved in writing a graduate thesis; thank you for understanding. To my Grandma Kerr: I will never forget that nobody loves me quite as much as you do. I love you, too, and I thank you for being in my life.

Also, my friends and mentors must be lavished with praise, especially Uwe Happek for giving me the opportunity to work in his lab; Marianne Happek for the congratulatory champagne; Carl Liebig for making sure I was full of coffee and the champagne; Long Pham for his merry pranks and the champagne, Bo "Linus" Wen for sharing deadlines with me during the past few months; Jay Fleniken for always helping to put things in perspective; Paul Schmidt for reminding of the value of a level head; Mkhulu Mathe for giving me a mountain of work and enthusiasm for the job; Raman Vaidyanathan for patiently getting me started in these studies; Kelly Patton for his refreshing sense of humor; Xiaolu "Jerry" Xi for her smile across my desk; Dr. Dennis for his time and for buying me espresso shots; Loris Magnani for his supportive words; and John Stickney for *everything* else.

To Kelly, I thank you for inspiring me with your fearlessness. I often refer to you as the hardest working person I've ever met, and your example will always urge me

to continue in spite hard times. I am certain that I could not have done this without you. I know that I can accomplish anything, because I've seen you do it more times than I can count.

Additionally, I would like to thank the city of Athens, this rotgut midnight town; I'd like to call it home. This place will always be Utopia to me, and I wouldn't trade my time here for anything. Some of my most precious memories include the time I spent at the Georgia Theatre, 40 Watt, and the Roadhouse. Also, my ears still have a satisfying ring from jamming with Matty Russo, Frank Teremy, Sean Schenker, Jonathan Sherman, Joe Guerzo, and Ed Connolly. All of you invited me into your circle music and in doing so, gave me the world. God bless you all and, I wish you great success. My roommates and friends throughout my tenure here, Darrin, Dan, Matthew, Stiles, Andrew, and Thomas; thanks, guys.

This list of incredible people who fill my life is endless, and I regret not being able to explicitly name everybody. So with a blanket statement of gratitude, I conclude this section with an invitation for you all to read my work.

Table of Contents

List of Figures

List of Tables

Chapter 1

Introduction

Thin films and nanostructures created by the method of electrochemical atomic layer epitaxy (EC-ALE), including InAs, In_2Se_3, and CdSe, have been characterized via energy gap measurements [1–5]. Measuring quantum confinement effects on semiconductor band gaps is a natural progression of our research of semiconductors, considering the ability of EC-ALE to grow thin films of semiconducting materials with atomic precision and/or with various templates. Quantum confinement of thin films created using the method of EC-ALE has not been rigorously studied until recently.

The creation and characterization of semiconductors with small physical dimensions has been very popular in the field of condensed matter, because knowledge of this physics is invaluable to manufacturers who try to satisfy an electronics market that demands increasingly smaller products. Generally, as the size of a semiconductor becomes comparable to and smaller than its exciton Bohr diameter, the energy gap of a semiconductor increases. In other words, the energy gap of a semiconductor becomes "blue-shifted" as its physical size decreases, and this phenomenon is known as quantum confinement [6,7].

As reported previously, nanowires of diameters ranging between 180 to 200 nm and $\sim$1 μm heights have been grown with EC-ALE using an etched polycarbonate membrane as a template [1]. However, these nanowires were too large to show a dramatic change in the energy gap. The obvious way that EC-ALE could grow

nanostructured materials is by varying semiconductor film thickness, thereby confining electron-hole pairs in one dimension. Alternatively, finer templating could be performed using the electron beam of a scanning electron microscope in conjunction with computer software to make nanometer sized EC-ALE molds out of poly(methylmethacrylate) (PMMA), better known by its various trade names including plexiglass and Lucite®. This capability has been recently installed at The University of Georgia and as of yet, has only been used to template vapor deposited materials for training purposes.

Generally, PbSe is an object of study because of its application in infrared and visible radiation detectors and emitters [6–14]. The choice of PbSe to study quantum confinement effects is based on its relatively large exciton Bohr radius (∼32 nm [8], ∼55 nm [12]), which makes the changes in energy gap as a function of crystal size more sensitive to variations of film thickness [9–12].

1.1 References

[1] R. Vaidyanathan, J. L. Stickney, S. M. Cox, S. P. Compton, U. Happek, J. Electroanal. Chem., In press, Available online 22 March 2003.

[2] B. H. Flowers, Jr., T. L. Wade, J. W. Garvey, M. Lay, U. Happek, J. L. Stickney, J. Electroanal. Chem., **524–525**, (2002) 273.

[3] T. L. Wade, L. C. Ward, C. B. Maddox, U. Happek, J. L. Stickney, Electrochem. Solid State Lett., **2**, (1999) 141.

[4] R. Vaidyanathan, Dissertation, The University of Georgia, 2003.

[5] P. R. Sprinkle, Dissertation, The University of Georgia, 2001.

[6] M. Fox, *Optical Properties of Solids*, (Oxford University Press, New York, 2001).

[7] Y. Wang, A. Suna, W. Mahler, R. Kasowski, J. Chem. Phys., **87**, (1987) 7315.

[8] R. Dalven, Infrared Phys., **9**, (1969) 141.

[9] S. Gorer, A. Albu-Yaron, G. Hodes, J. Phys. Chem., **99**, (1995) 16442.

[10] E. A. deAndrada e Silva, Phys. Rev. B, **60**, (1999) 8859.

[11] A. D. Andreev, E. V. Kolobkova, A. A. Lipovskii, J. App. Phys., **88**, (2000) 750.

[12] I. Kang, F. W. Wise, J. Opt. Soc. Am. B, **14** (1997) 1632.

[13] M. Pinczolits, G. Springholz, G. Bauer, App. Phys. Lett., **73**, (1998) 250.

[14] H. Krenn, S. Yuan, N. Frank, G. Bauer, Phys. Rev. B, **57**, (1998) 2393.

Chapter 2

Electrochemical Atomic Layer Epitaxy

Electrochemical atomic layer epitaxy (EC-ALE) has been referred to as a sophisticated form of bumper plating, using a technique known as underpotential deposition (UPD), which is a surface limited reaction, to grow semiconductor films one atomic layer at a time at room temperature. Binary compound semiconductor films are grown by alternately depositing atomic layers of the constituent elements the compound. This layer by layer growth of a compound constitutes epitaxial formation of semiconductor thin films [1–6].

The decided advantage of EC-ALE over alternative epitaxial methods, namely molecular beam epitaxy (MBE) and vapor phase epitaxy (VPE), is the ability to form a single layer of a compound at room temperature and atmospheric pressure by controlling the deposition potential. MBE and VPE can form compound monolayers by controlling thermal factors, however high temperature deposition can promote interdiffusion between atomic layers. EC-ALE's ability to form monolayer deposits of elements in a condensed phase at room temperature would therefore be advantageous for layering dopants in between pure semiconductor layers or for forming superlattice crystal structures of semiconductors, for example [1,5,6].

2.1 UPD

UPD exploits the potential that causes specific atoms in solution to deposit onto the surface of an electrode but does not cause the same atoms to deposit onto themselves.

Theoretically, no more than one atomic layer, defined as one monolayer, of specific atoms will be deposited at this potential [1].

The specific UPD potential for a substance is determined by cyclic voltammetry. Figure 2.1 shows the cyclic voltammogram of the Au electrode in a pH 5.5 solution of 0.3 mM SeO_2, 50 mM CH_3COONa, and 0.1 M $NaClO_4$. The potential across the Au working electrode and the reference electrode is measured and made to change at a constant rate of $-5\,\mathrm{mV\,s^{-1}}$ by controlling the current through the auxiliary and the working Au electrode. The current measured through the auxiliary and working electrode is then plotted as a function of the measured potential between the working electrode and the reference electrode, and peaks at specific potentials are analyzed. Small peaks in this I–V curve are noted before a final large peak, which corresponds to bulk deposition of semiconductor. A preceding small peak corresponds to the deposition potential at which less than one atomic layer is deposited, hence the name underpotential. At the end of the negative potential ramp, the potential across the working electrode and auxiliary electrode is ramped towards positive potentials, which reveals current peaks that correspond to the stripping of the deposited semiconductor. The actual value of underpotential that is chosen to begin deposition of the first elemental layer corresponds to a voltage between the underpotential and bulk deposition peaks. For the case of Pb displayed in Figure 2.1, the underpotential value was determined to be $-0.200\,\mathrm{V}$. This value is coincident with the value determined for Se by Figure 2.2 [6].

2.2 EC-ALE Apparatus

The electrochemical cell used to deposit semiconductor films is made of a plexiglass frame designed to promote laminar flow and uses a Au working electrode, an indium tin oxide (ITO) auxiliary electrode, and a Ag/AgCl reference electrode

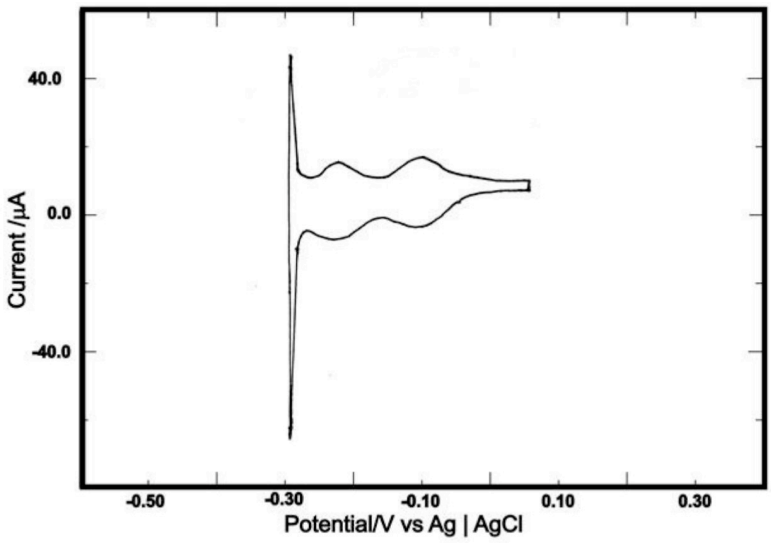

Figure 2.1: The cyclic voltammogram of the EC-ALE electrochemical cell containing 0.2 mM $Pb(ClO_4)_2$, 50 mM CH_3COONa, and 0.1 M $NaClO_4$. The UPD potential for deposition of Pb on Au was determined to be -0.200 V [6].

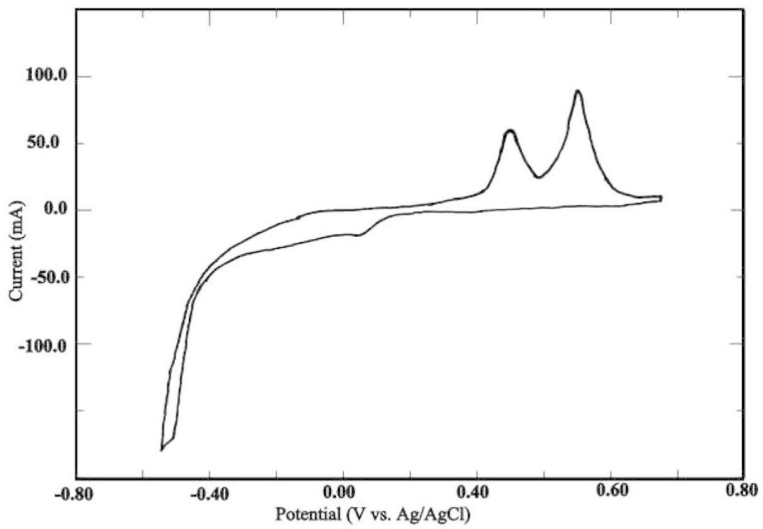

Figure 2.2: The cyclic voltammogram of the EC-ALE electrochemical cell containing 0.2 mM SeO_2, 50 mM CH_3COONa, and 0.1 M $NaClO_4$. The UPD potential for deposition of Se on Au was determined to be -0.200 V [6].

(Figure 2.3). The cell is mounted on top of a plexiglass box, which houses the cell's chemical delivery system of computer-controlled peristaltic pumps and respective valves. To avoid oxygen contamination, the pump box and all of the aqueous chemical containers and tubing that feed the cell are purged constantly with nitrogen. Potentials are applied to the electrodes using a computer-controlled potentiostat, and was interfaced with the program Lab View^{TM} (National Instruments Co.) [1–6].

2.3 Substrates

All EC-ALE-borne thin films studied in this thesis are deposited on Au substrates. To make a substrate, a standard glass microscope slide is etched in a solution of HF (15% by volulme in H_2O), rinsed with purified water, and mounted in a vapor depositor, which is then evacuated and heated to 400^o C. A preliminary 3 nm layer of Ti is deposited on the glass followed by a 600 nm layer of Au. Titanium's ability to adhere to glass is much greater than that of Au, which makes it useful as a sublayer for the Au substrate. Shown in Figure 2.4, the deposition temperature causes the Au to form [111] plateaus that are roughly 200 to 600 nm wide, the flat portions of which reflect the [111] plane of Au's Bravais lattice structure. After a Au covered microscope slide is removed from the vapor deposition chamber, it is dipped in HNO_3 again, then rinsed in nanopure water, and dried with a stream of nitrogen gas. To minimize small (< 50 nm) grains on the Au plateaus, the substrates are manually annealed with a H_2 flame [1,6].

2.4 PbSe

To grow PbSe compound layers with EC-ALE, aqueous solutions of the constituent elements were prepared with reagent grade or better chemicals as follows: For Pb, 0.2 mM $Pb(ClO_4)_2$ (Alfa Aesar, Ward Hill, MA) was prepared with a pH of 5.5

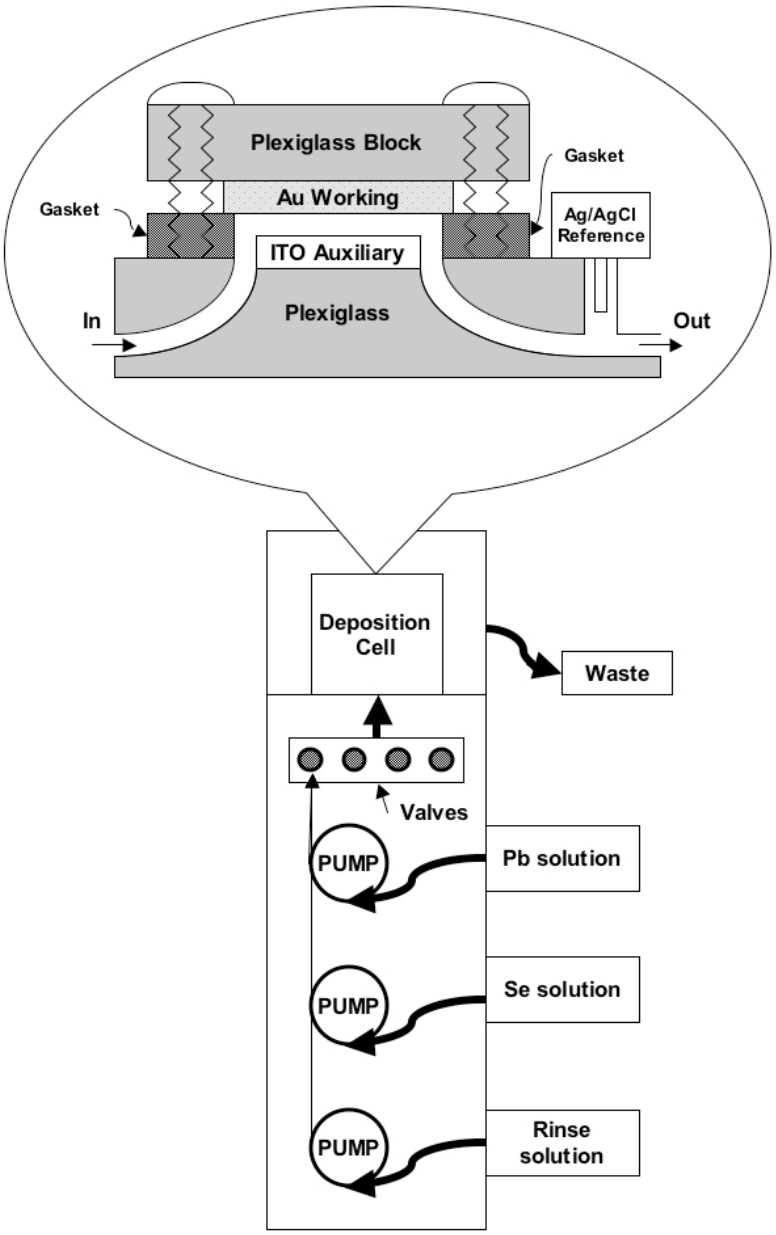

Figure 2.3: The EC-ALE apparatus consisting of peristaltic pumps and valves inside a nitrogen purged plexiglass box. The magnification illustrates the electrochemical cell used to deposit thin film semiconductors onto a Au substrate.

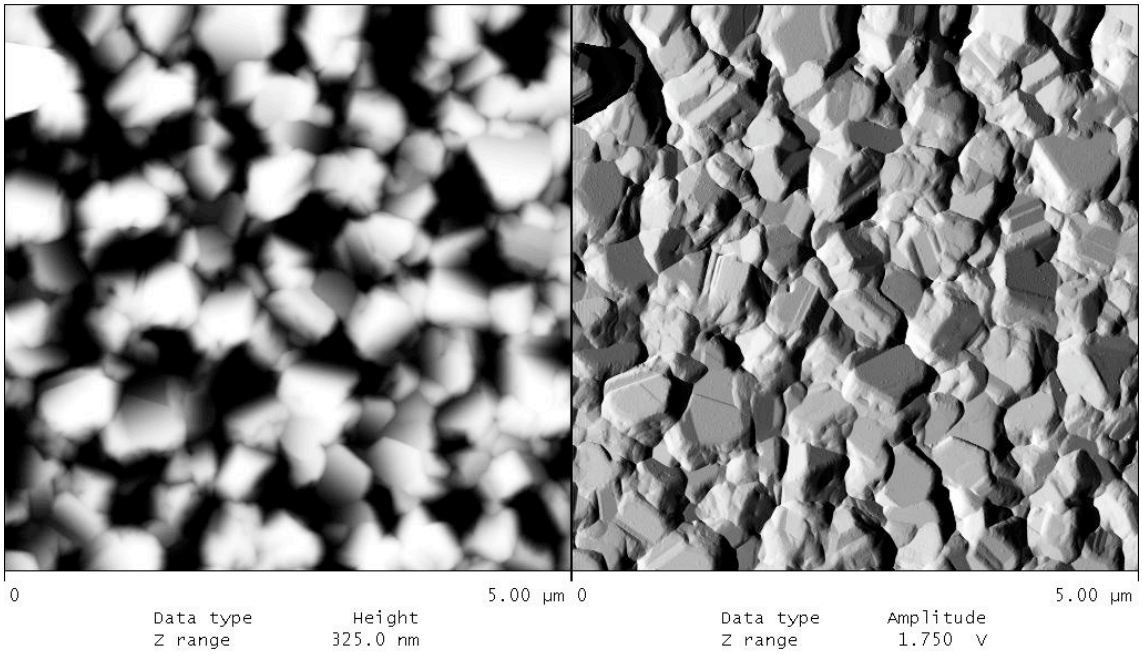

Figure 2.4: AFM image of an ideal Au substrate vapor deposited on Ti on glass (Left: Topographic data; Right: Tip amplitude data). Clearly visible are the Au plateau formations reflecting the [111] plane of the Au Bravais lattice structure.

and buffered with 50.0 mM $CH_3COONa\ 3H_2O$ (J. T. Baker). Finally, a supporting electrolyte of 0.1 M $NaClO_4$ (Fischer Scientific, Pittsburgh, PA) was added. A pH 5.5 solution of 0.2 mM SeO_2 (Alfa Aesar, Ward Hill, MA) was prepared with the same buffer as the Pb solution and with the same supporting electrolyte. All water that was used came from a Nanopure® water filtration system (Barnstead, Dubuque, IA) [6].

Deposition of a PbSe thin film is done by alternately depositing Pb and Se layers of atoms on the Au working electrode. First, the electrochemical cell is filled with the Pb solution at a potential of −0.200 V (UPD value determined by cyclic voltammetry explained in Section 2.1) for 25 seconds followed by a 0.1 M $NaClO_4$ rinse solution of pH 5.5 for 2 seconds. Then, the cell is filled with the Se solution and held at a potential of −0.200 V for 15 seconds followed again by the rinse solution. This procedure constitutes one cycle or one compound monolayer of PbSe [6].

After the first cycle, the deposition potentials need to be changed because the nature of the substrate changes. The potential of −0.200 V is optimum for the deposition of Pb on Au and Se on one monolayer of Pb on Au, but following cycles require the deposition potential to be optimum for an ever-thickening substrate of PbSe. An empirical model of the change in deposition potential required to form quality films was devised experimentally and is defined by the quantity:

$$c = \frac{(V_\mathrm{f} - V_\mathrm{i})}{\ln N} \tag{2.1}$$

called the *incremental coefficient*, where V_f is the final deposition potential, V_i is the initial deposition potential, and N is the number of cycles performed to create the film. Using the incremental coefficient c, the equation:

$$V_\mathrm{f} = V_\mathrm{i} + c \ln N \tag{2.2}$$

governs the computer-controlled change in potential as the film becomes thicker. Normally, ramping the deposition potential is only required for the first 10 to 30

cycles of the EC-ALE process. Specifically for PbSe, the number of cycles, N, in Equations 2.1 and 2.2 was experimentally found to be 10. After ten layers of PbSe is deposited, the depositon potentials were kept constant [1].

A coverage factor, the fraction of the substrate area that is covered with a monolayer of Pb or Se ions, can be calculated from coulometry using the current versus time traces of each deposition cycle. Given ideal growth conditions, the coverage factor corresponding to each layer of Pb and Se, respectively, should equal 1.00. To estimate the thickness of a multi-cycle semiconductor film, the average coverage factor of each layer can be multiplied by the expected theoretical film thickness. In this study of PbSe, the aforementioned method was used to estimate film thickness, because more precise methods were unavailable (Table 3.4).

2.5 References

[1] J. L. Stickney, *Advances in Electrochemical Science and Engineering*, R. C. Alkire and D. M. Kolb, Eds., (Interscience Publishers, John Wiley and Sons, Inc., New York, 2003).

[2] R. Vaidyanathan, J. L. Stickney, S. M. Cox, S. P. Compton and U. Happek, J. Electroanal. Chem., In press, Available online 22 March 2003.

[3] B. H. Flowers, Jr., T. L. Wade, J. W. Garvey, M. Lay, U. Happek and J. L. Stickney, J. Electroanal. Chem., **524–525**, (2002) 273.

[4] T. L. Wade, L. C. Ward, C. B. Maddox, U. Happek and J. L. Stickney, Electrochem. Solid State Lett., **2**, (1999) 141.

[5] T. L. Wade, R. Vaidyanathan, U. Happek and J. L. Stickney, J. Electroanal. Chem., **500**, (2001) 322.

[6] R. Vaidyanathan, Dissertation, The University of Georgia, 2003.

Chapter 3

Characterization of Semiconducting Thin Films Created Using EC-ALE

3.1 Direct Energy Gap

The formation of bands in a crystal can be treated by the tight-binding model of solids, which states that electronic bands form from the broadening of the discrete outer electronic shells of individual atoms caused by decreasing interatomic separation. At absolute zero temperature, electrons fill the bands up to an energetic level known as the *Fermi energy*. In conductors, the highest occupied band is only partially filled, which allows electron mobility, and contains the Fermi level. However, the highest occupied band in semiconductors, the *valence band*, is completely filled and allows no electron mobility. Electrons from the valence band may be excited in some way to move to a nearby empty band known as the *conduction band*, so called because electrons there are free to be accelerated and thereby conduct electricity. The energetic distance between the highest level of the valence band and the lowest level of the conduction band is known as the *energy gap*. In between the conduction and valence bands resides the Fermi level of a semiconductor [1].

An electron in an atom can be excited from a low energy state to a high energy state by absorbing a photon. If the energy of an exciting photon is $h\nu$, and the energies of the low energy state and the high energy state are E_1 and E_2, respectively, then:

$$h\nu = E_2 - E_1 \tag{3.1}$$

and energy is conserved. In a solid, this picture of electron excitation by photon absorption is complicated by the formations of continuous electronic bands. Electronic transitions induced by a photon of energy $h\nu$ from the valence band of energy E_{v} to the conduction band of energy E_{c} in a solid semiconductor are still governed by the conservation of energy:

$$h\nu = E_{\mathrm{c}} - E_{\mathrm{v}} \tag{3.2}$$

and E_{c} can range the width of the band, the minimum value of $(E_{\mathrm{c}} - E_{\mathrm{v}})$ being the energy gap, E_{g}. Therefore, the photon energy causing an electronic interband transition must exceed the energy of the gap between the valence and conduction bands; $h\nu > E_{\mathrm{g}}$ [1].

An electron that is excited from the valence band to the conduction band leaves behind a *hole* in the valance band, thus creating an electron-hole pair. A hole is essentially the absence of an electron, but a hole is formally treated as having effective charge and an effective mass [1].

The semiconductor band structure is divided into Brillouin zones defined by the reciprocal lattice vectors, $\mathbf{K}$, of the the crystal, and the energy levels can be plotted as functions in k-space. An electron's momentum is defined by the reciprocal lattice vectors of the crystal as $\hbar\mathbf{K}$, and momentum must be conserved during an electron's absorption of a photon and subsequent interband transition according to the equation:

$$\hbar\mathbf{K}_{\mathrm{f}} - \hbar\mathbf{K}_{\mathrm{i}} = \hbar\mathbf{k} \tag{3.3}$$

where the change in the electron's momentum after changing states is equal to the momentum of the exciting photon. The magnitude of the photon's wavevector is $2\pi/\lambda$, where λ is the wavelength of the photon. Therefore, the photon's momentum is generally orders of magnitude smaller than the the electron's momentum in either

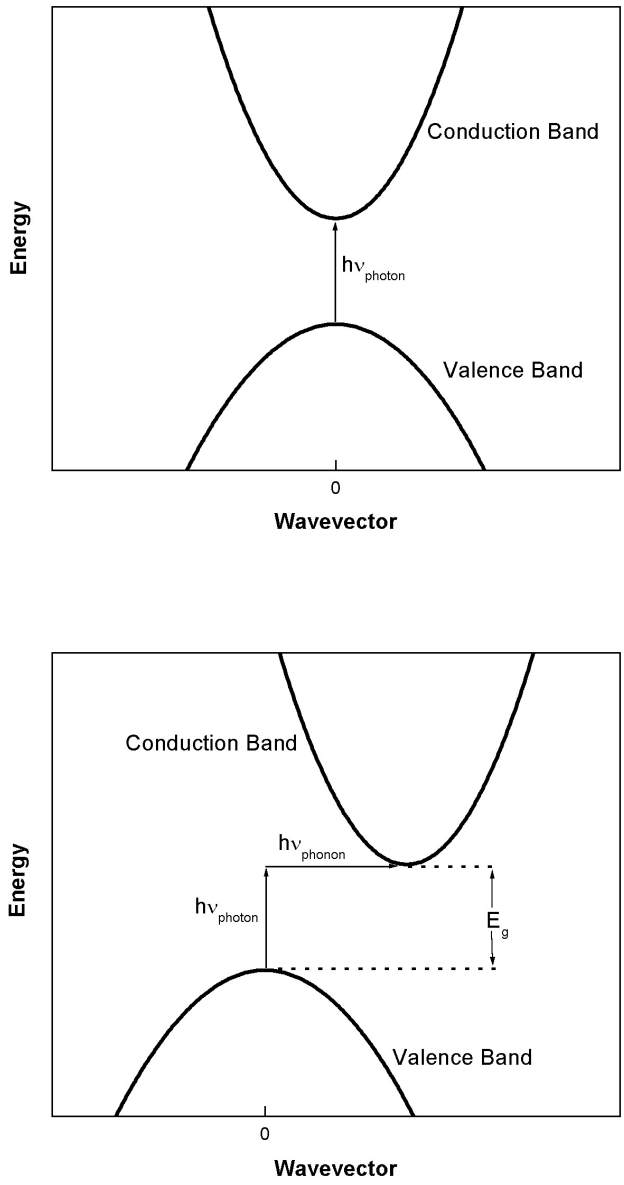

Figure 3.1: Idealized direct (top) and indirect (bottom) transitions in one dimensional k-space.

state, and the wavevectors of the electron in the initial and final states are approximately equal. In other words, $\Delta k = 0$ during the electron's change in state, and this characteristic defines a *direct* transition (Fig. 3.1). Thus, the energy gap separating the valence and conduction bands at the same point in k-space is referred to as the *direct energy gap* if it can be bridged by an electron with absorbed photonic energy. An *indirect* transition in a semiconductor is also an intensely studied property of semiconductors. An indirect interband electronic transition, where $\Delta k \neq 0$ in k-space, involves the electronic absorption of a photon and a phonon to conserve momentum (Fig. 3.1). Silicon and Germanium are both indirect gap semiconductors that are of great commercial significance [1,2].

Taking the zero value of energy to be at the top of the valence band for a semiconductor, the energy of an electron in the conduction band can be described using the nearly free electron model by:

$$E_{\mathrm{e}} = E_{\mathrm{g}} + \frac{\hbar^2 k^2}{2m_{\mathrm{e}}^*} \tag{3.4}$$

where the second term is the electron's kinetic energy, and m_{e}^* is the effective mass of the electron. Similarly, the energy of the hole can be written:

$$E_{\mathrm{h}} = -\frac{\hbar^2 k^2}{2m_{\mathrm{h}}^*} \tag{3.5}$$

where m_{h}^* is the hole's effective mass, and E_{c} and E_{h} describe the dispersion of the bands of the electron and hole, respectively, in k-space. The effective masses, therefore, can be calculated from the curvature of the dispersion with respect to k, which is parabolic for small k. The *fundamental energy gap* of a semiconductor occurs at the value of k where both the valence band and the conduction band have the least energetic separation [1,2].

The difference between the photon energy and the energy gap is equal the combined energies of the electron and hole:

$$h\nu - E_{\mathrm{g}} = \frac{\hbar^2 k^2}{2m_e^*} + \frac{\hbar^2 k^2}{2m_h^*} \tag{3.6}$$

which is a restatement of equation 3.2 using equations 3.4 and 3.5. The photon energy $h\nu$ absorbed by an electron must be greater than or equal to the energy gap, E_{g}, to cause an interband transition. Using this formalism, the electronic transitions within a semiconductor crystal can be found by measuring photon absorption [1,2]

3.2 Quantum Confinement Effects on the Direct Energy Gap

The direct energy gap of a semiconductor changes as dimensional size becomes smaller, and this effect is referred to as quantum confinement. Size dependent quantum effects can be used to tune the electrical properties of different semiconductors in the same spirit as the intentional doping of silicon to engineer semiconductors with desirable properties. Therefore, modeling the effects of quantum confinement in different materials is necessary for their practical application [3].

According to the Heisenberg Principle:

$$\Delta x \Delta p_x \geq \frac{\hbar}{2} \tag{3.7}$$

a particle confined to a region in the x-direction, Δx, will have uncertainty in its momentum, Δp_x. The approximate expression for the particle's momentum is given by the equation:

$$\Delta p_x \sim \frac{\hbar}{\Delta x} \tag{3.8}$$

Calculating the kinetic energy of the particle that is confined in the x-direction:

$$E \sim \frac{(\Delta p_x)^2}{2m} \tag{3.9}$$

will give a value of the *confinement energy* of the particle:

$$E_{\text{confinement}} \sim \frac{\hbar^2}{2m(\Delta x)^2} \tag{3.10}$$

If the particle's thermal kinetic energy in the x-direction is less than or equal to the confinement energy, then quantum size effects become apparent [1].

The change in the direct energy gap caused by spatial particle confinement in one dimension is often modeled by the simple particle-in-a-box model of quantum mechanics. This model is based on the nearly free electron model described in Section 3.1. When a photon excites an electron of the valence band to the conduction band of a semiconductor, a hole, or lack of an electron, is created in the valence band. The excited electron and corresponding hole can be modeled as a single entity, called an exciton, where the electron and hole orbit around each other. The exciton can be modeled like the hydrogen atom with an effective reduced mass of μ defined by the equation:

$$\frac{1}{\mu} = \frac{1}{m_e^*} + \frac{1}{m_h^*} \tag{3.11}$$

where m_e^* and m_h^* are the effective masses of the electron and the hole, respectively [1].

Consider the electron-hole pair of reduced mass μ to be confined to a one-dimensional quantum well of width L centered about the origin with infinite potential walls. The one-dimensional Schrödinger equation in this case is:

$$-\frac{\hbar^2}{2\mu}\frac{d^2}{dx^2}\psi + V(x)\,\psi = E\psi \tag{3.12}$$

where the potential of the electron-hole pair is: $V(x) = -e^2/(4\pi\epsilon_\infty\epsilon_\text{o}\,x)$, ϵ_∞ is the dielectric constant of the semiconductor, ϵ_o is the permittivity of free space, e is the charge of a free electron, and x is the position of the electron-hole pair. This can be diagonalized to yield the eigenvalue:

$$E = \frac{\hbar^2\pi^2 n^2}{2\mu L^2} - \frac{1.8e^2}{(4\pi\epsilon_\infty\epsilon_\text{o})L} \tag{3.13}$$

where L is the width of the potential well reflecting the size of the semiconductor crystal. Taking $n = 1$ for the first excited state of the electron-hole pair, Equation 3.6 and Equation 3.13 are approximately equal (neglecting the potential term), because the minimum allowed deBroglie wavelength of the electron-hole pair is defined by its crystal size by the relation: $\lambda_{\min}/2 = L$. Therefore, conservation of energy requires the energy gap to increase if the size, L, of the crystal becomes smaller than half of $\lambda_{\min}$. The size of a semiconductor before the energy gap must change from its bulk value is modeled after the Bohr radius of the hydrogen atom by the equation:

$$R_{\mathrm{B}} = \frac{\hbar^2(4\pi\epsilon_\infty\epsilon_{\mathrm{o}})}{\mu e^2} \tag{3.14}$$

Effectively, the energy gap of the semiconductor will increase as $\lambda_{\min}$ of the electron-hole pair becomes smaller than R_{B}, the exciton Bohr radius of the semiconductor. Therefore, the eigenvalue E can be interpreted as ΔE_{g}, or the change in the energy gap of the material from its bulk value as L becomes smaller than the Bohr diameter of the electron-hole pair, so that:

$$E_{\mathrm{g}} = E_{\mathrm{g,bulk}} + \Delta E_{\mathrm{g}} = E_{\mathrm{g,bulk}} + \frac{\hbar^2\pi^2}{2\mu L^2} - \frac{1.8e^2}{4\pi\epsilon_\infty\epsilon_{\mathrm{o}}L} \tag{3.15}$$

and the change in E_{g} as a function of crystal size can be predicted. This treatment is known as the *effective mass approximation* or the *parabolic effective mass model* [1,4].

Wang *et al.* [4] report an alternative model that accurately predicts the change in energy gap of the lead salts in general as a function of size in the nanometer range, and this model was devised in response to the apparent nonparabolicity of the conduction and valence bands of PbSe near the k-value of the energy gap. Dubbed the *hyperbolic band model*, this alternative model treats the energy in k-space of the conduction and valence bands as a hyperbolic function. Also, it treats the effective

electron and hole masses as isotropic; the same in all directions of k-space:

$$E_{\mathrm{g}} = \sqrt{E_{\mathrm{g,bulk}}^2 + 4\frac{\hbar^2\pi^2}{2m^*L^2}\,E_{\mathrm{g,bulk}}} \tag{3.16}$$

where L is semiconductor size.

Effective mass values for the electon and hole that are reported by Pankove [6] correspond to three directions in k-space. The longitudinal effective mass, m_l, applies to one direction and the transverse effective mass, m_t, applies to two other separate directions. The effective mass reported as a single value is the weighted average of the longitudinal and transverse effective masses; $(2m_t + m_l)/3$.

Using the values of effective electron and hole masses described above, Wang *et al.* [4] employ a singular isotropic average effective mass to suit the hyperbolic band model using the equation:

$$\frac{1}{m^*} = \frac{1}{2}\left(\frac{1}{m_{\mathrm{e}}^*} + \frac{1}{m_{\mathrm{h}}^*}\right) \tag{3.17}$$

where m^* is used instead of reduced effective mass, μ, to calculate the hyperbolic band model.

3.3 Optical Methods for Determining the Direct Energy Gap of a Thin Film Semiconductor

The transmittance spectra of thin film semiconductors can be analyzed to determine their energy gaps. Transmittance spectra can be measured using Fourier transform infrared spectroscopy or dispersive spectroscopy methods. The transmittance through a thin film is defined as the wavelength-dependent intensity, I, of radiation transmitted through the material divided by the wavelength-dependent incident intensity, I_{o}, transmitted through space. A transmittance plot is defined as I/I_{o} versus $h\nu$. The absorption coefficient $\alpha(h\nu)$ can be determined from the the relative intensity, I/I_{o}, of the transmittance spectra using Beer's equation:

$$I = I_{\mathrm{o}}\,(1-R)^2\,e^{-\alpha d} \tag{3.18}$$

where R is the reflectivity of the material, and d is the thickness of the thin film. The factor $(1 - R)^2$ is actually the product of $(1 - R_1)$ and $(1 - R_2)$, where R_1 and R_2 are the reflectivities of the first space-film interface and the second film-space interface, respectively. In this treatment, R_1 and R_2 are taken to be equal, thus $R_1 = R_2 = R$ [1].

To deduce the energy gap from transmittance spectra by studying photon absorption, the energy dependence of the absorption coefficient can be found by considering the perturbation effects of light radiation on an electron. The Hamiltonian for the electron subject to the electromagnetic field of light is:

$$H = \frac{\mathbf{p}^2}{2m_\mathrm{e}} + V(\mathbf{r}) + e\,(\mathbf{r} \cdot \mathbf{E}_\mathrm{ph}) \tag{3.19}$$

where $\mathbf{p}$ is the momentum of the electron before photon interaction, m_e is the mass of the electron, $V(\mathbf{r})$ is the potential energy of the electron, $-e$ is the charge of the electron, $\mathbf{E}_\mathrm{ph}$ is the electric field of the photon, and $\mathbf{r}$ is the vector position of the electron. The first two terms in the Hamiltonian describe the electron before interaction with the photon, and the third term is the perturbation due to the photon, which is called H'. The quantum mechanical transition rate, $W_{\mathrm{i}\to\mathrm{f}}$, that governs the excitation of an electron from some initial state, i, to a final state, f, is defined by Fermi's golden rule:

$$W_{\mathrm{i}\to\mathrm{f}} = \frac{2\pi}{\hbar}\,|M|^2\,g(h\nu) \tag{3.20}$$

where $g(h\nu)$ is the joint density of states. M is a matrix element defined by the equation:

$$M = \int \psi_\mathrm{f}^*(\mathbf{r})\,H'(\mathbf{r})\,\psi_\mathrm{i}(\mathbf{r})\,d^3\mathbf{r} \tag{3.21}$$

where $\psi_\mathrm{f}(\mathbf{r})$ and $\psi_\mathrm{i}(\mathbf{r})$ are the wavefunctions of the electron in the final and initial states, respectively. The density of states, $g(E)$, describes the intraband electron distibution in a band, while the joint density of states, $g(h\nu)$, is evaluated at the

energy of the absorbed photon responsible for the electron-hole pair. For an electron in a parabolic band, the density of states in the band can be calculated to be:

$$g(E) \;=\; \frac{1}{2\pi^2}\,\frac{(2\mu)^{\frac{3}{2}}}{\hbar^3}\,(E)^{\frac{1}{2}} \tag{3.22}$$

Recalling Equation 3.6, the absorbed photon of energy $h\nu$ must be greater than or equal to the energy gap to excite an electron into the conduction band. Therefore, the joint density of states evaluated at the energy of the absorbed photon is given by Equation 3.22 with E equal to $h\nu - E_{\mathrm{g}}$:

$$g(h\nu) \;=\; \frac{1}{2\pi^2}\,\frac{(2\mu)^{\frac{3}{2}}}{\hbar^3}\,(h\nu - E_{\mathrm{g}})^{\frac{1}{2}} \tag{3.23}$$

where for photon energies less than E_{g}, the joint density of states equals zero. From Fermi's golden rule, the absorption rate is proportional to the joint density of states:

$$W_{\mathrm{i}\to\mathrm{f}} \;\propto\; g(h\nu) \tag{3.24}$$

which implies that the absorption coefficient is also proportional to $g(h\nu)$:

$$\alpha(h\nu) \;\propto\; g(h\nu) \;=\; \frac{1}{2\pi^2}\,\frac{(2\mu)^{\frac{3}{2}}}{\hbar^3}\,(h\nu - E_{\mathrm{g}})^{\frac{1}{2}} \tag{3.25}$$

This equation allows for the measurement of a semiconductor's direct band gap from the absorption coefficient [1].

Assuming parabolic bands near the electronic transition point in k-space, the practical equation for α as a function of photon energy is:

$$\alpha(h\nu) \;=\; A\,(h\nu - E_{\mathrm{g}})^{1/2} \tag{3.26}$$

where A is the proportionality constant, and E_{g} is the direct energy gap [1,6]. As photon energy becomes greater than E_{g}, $\alpha(h\nu)$ should increase like $(h\nu - E_{\mathrm{g}})^{1/2}$. This corresponds to a linear region within a plot of α^2 *vs.* $h\nu$. Extrapolating a line from the linear region to $\alpha = 0$ would intercept the $h\nu$-axis at the value of E_{g} [1].

3.3.1 Experimental determination of EC-ALE semiconductor energy gaps

Energy gaps of the ECALE thin films were calculated from transmittance spectra measured by Fourier transform infrared spectroscopy (Bruker FTS-66v, Bruker Optics, Inc.). Sources used were a Tungsten lamp and a Globar® for near and mid-infrared wavelength ranges, respectively. Mercury cadmium telluride, InSb, Ge, and Si detectors were used for specific middle to near infrared radiation ranges. CaF_2 and quartz beamsplitters were used for the middle and near infrared ranges, respectively [5].

Because the films were grown on an opaque Au substrate, transmittance measurements were performed by passing the source radiation through a reflection apparatus that exploited the Brewster angle, θ_{B}, of the semiconductor material. Polarized such that its electric field vectors are oriented parallel to plane of incidence, incident radiation at the Brewster angle transmits through the semiconductor and reflects off of the gold substrate. Ideally, no radiation is reflected from the surface of the semiconductor incident at the angle defined as:

$$\theta_{\mathrm{B}} = \tan^{-1}(\frac{n_{\mathrm{sc}}}{n_{\mathrm{o}}}) \tag{3.27}$$

where n_{sc} is the index of refraction of the semiconductor, and n_{o} is the index of refraction of the medium through which the incident light travels to the semiconductor interface, which is usually ambient air or an environment depressurized to $\sim 10^{-3}$ bar where n_{o} is taken to equal to one [5].

Using equation 3.18, $R \sim 0$, so that:

$$\alpha d = -\ln \frac{I}{I_{\mathrm{o}}} \tag{3.28}$$

transmittance data could be converted to absorption plots for energy gap analysis. The value d was defined as the distance that the transmitted radiation travelled

through the semiconductor material and is calculated using the equation:

$$d = \frac{2t}{\sqrt{1 - \frac{\sin^2(\theta_{\mathrm{I}})}{n^2}}} \tag{3.29}$$

where t is the thickness of a film, and θ_{I} is the incident radiation angle equal to θ_{B}. An exact calculation of d is impeded by the lack of direct thickness measurements of the thin films. Instead of a direct measurement of t, the theoretically calculated thickness of the thin films is used. In the case of PbSe, the films are thought to grow in the [111] direction of the rock salt crystal structure with lattice constant, $a = 6.124\,\text{Å}$, giving each compound layer a thickness of $a\sqrt{3}/3 = 3.536\,\text{Å}$ [6]. Multiplying the number of EC-ALE growth cycles by the theoretical thickness of each [111] compound layer gives an estimate of the thickness of each film.

Table 3.1: CdSe energy gap data of absorption spectra shown in Figures 3.2, 3.3, 3.4, and 3.5. Samples that did not exhibit a measurable energy gap have an X in the energy gap column.

Sample	E_g **[eV]**	**Deposition Potentials [V]**
CdSe 3/06/03	1.740 ± 0.018	Cd: −0.300 → −0.550; Se: −0.300 → −0.580
CdSe 3/21/03	1.718 ± 0.026	Cd: −0.300 → −0.700; Se: −0.300 → −0.700
CdSe 3/24/03	1.725 ± 0.025	Cd: −0.300 → −0.650; Se: −0.300 → −0.650
CdSe 3/28/03-1	1.717 ± 0.015	Cd: −0.300 → −0.650; Se: −0.300 → −0.675
CdSe 3/28/03-2	1.722 ± 0.024	Cd: −0.300 → −0.650; Se: −0.300 → −0.625
CdSe 3/30/03	1.701 ± 0.017	Cd: −0.300 → −0.675; Se: −0.400 → −0.650
CdSe 3/31/03	1.719 ± 0.007	Cd: −0.300 → −0.625; Se: −0.300 → −0.625
CdSe 3/18/03	X	Cd: −0.300 → −0.800; Se: −0.280 → −0.700
CdSe 3/20/03	X	Cd: −0.300 → −0.800; Se: −0.300 → −0.800
CdSe 4/01/03	X	Cd: −0.300 → −0.600; Se: −0.350 → −0.600

3.3.2 CdSe

CdSe is a II-VI compound semiconductor with a reported energy gap of $\sim 1.74\,\text{eV}$ at $300\,\text{K}$ [6], which is easily measured using optical absorption data. The exciton Bohr radius of CdSe is $\sim 3\,\text{nm}$ [3], but size-quantization effects of EC-ALE CdSe films were not tested in this thesis. Their inclusion is meant to illustrate the effectiveness of Equation 3.26 in measuring the band gap of a thin film semiconductor on an opaque substrate.

The solutions used to grow CdSe for this project were prepared with reagent grade or better chemicals. For deposition of Cd layers, 0.5 mM $CdSO_4$ (Alfa Aesar, Ward Hill, MA) of pH 5.0 with a supporting electrolyte of 0.5 M Na_2SO_4 (Fischer Scientific, Pittsburgh, PA) was prepared. For deposition of Se layers, 0.5 mM SeO_2 (Alfa Aesar, Ward Hill, MA) of pH 5.0 with a supporting electrolyte of 0.5 M Na_2SO_4 was prepared. No complexing agents or buffers were used to prepare either

of the before-mentioned solutions. All pH values were adjusted using H_2SO_4 (Fischer Scientific, Pittsburgh, PA).

One cycle of CdSe is defined as the deposition a Cd monolayer followed by the deposition of a Se monolayer. A blank solution of 0.5 M Na_2SO_4 of pH 5.0 was used to rinse the cell between cycles. Deposition potential ramping was performed up to 30 cycles according to Equation 2.2, after which the deposition potential was kept constant up to the 200^{th} cycle. All films reported here are 200 cycles thick. The initial and final deposition potentials are listed in Table 3.1 for each sample.

Table 3.1 shows the values of band gap determined by FTIR measurements for each of the films and Figures 3.2, 3.3, 3.4, and 3.5 show how the energy gaps were determined from absorption spectrum using Equation 3.26. These results can be useful in determining optimal deposition potentials. Sample CdSe 3/06/03 exhibits an energy gap of $1.740 \pm 0.018\,\text{eV}$, which agrees with the value reported for bulk CdSe at 300 K [6]. This result may indicate that the sample was grown under optimal conditions. The fact that samples CdSe 3/18/03, 3/20/03, and 4/01/03 have absorption spectra that lack identifiable absorption edges may indicate that those films are not characteristic of epitaxial CdSe. Additionally, the surface features of these films were sufficiently rough as to prohibit quality imaging with the atomic force microscope. The relevance of this observation is explored further in Section 3.4.

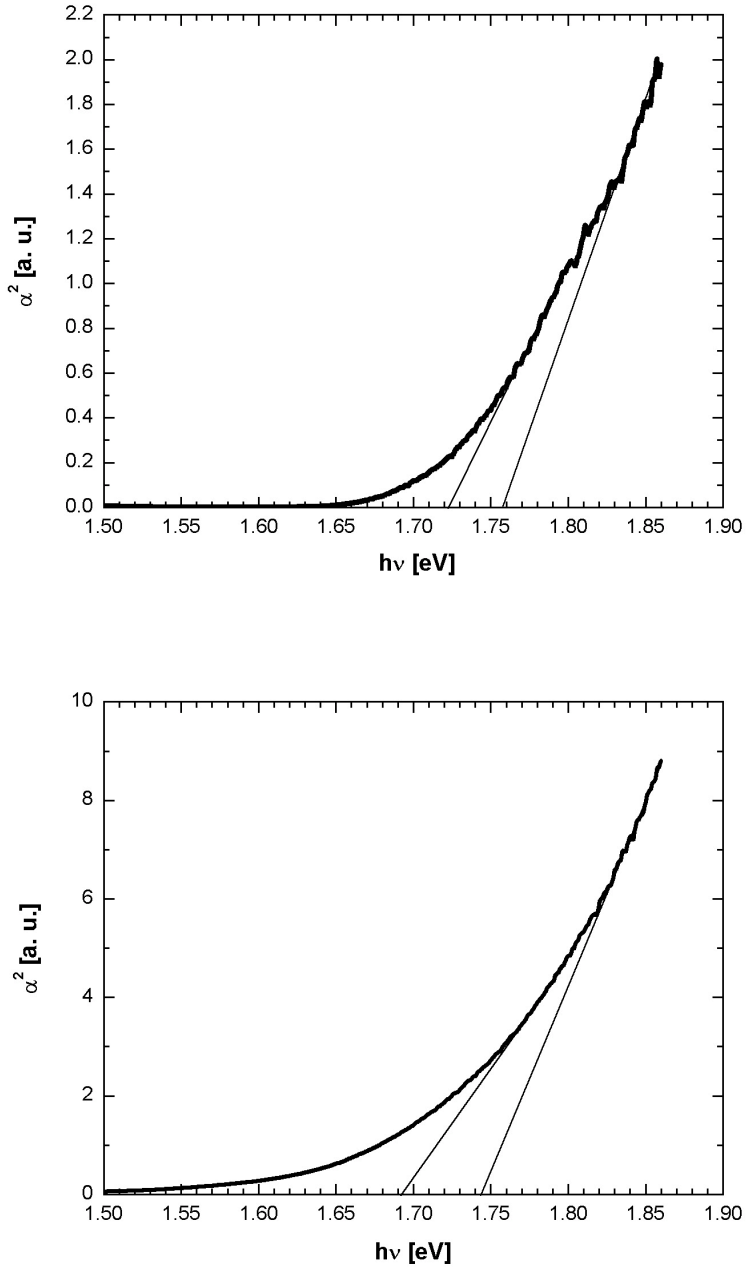

Figure 3.2: α^2 spectra of CdSe 3/06/03 (top) and CdSe 3/21/03 (bottom). Extrapolation lines intersect the $h\nu$-axis at the energy gap according to Equation 3.26.

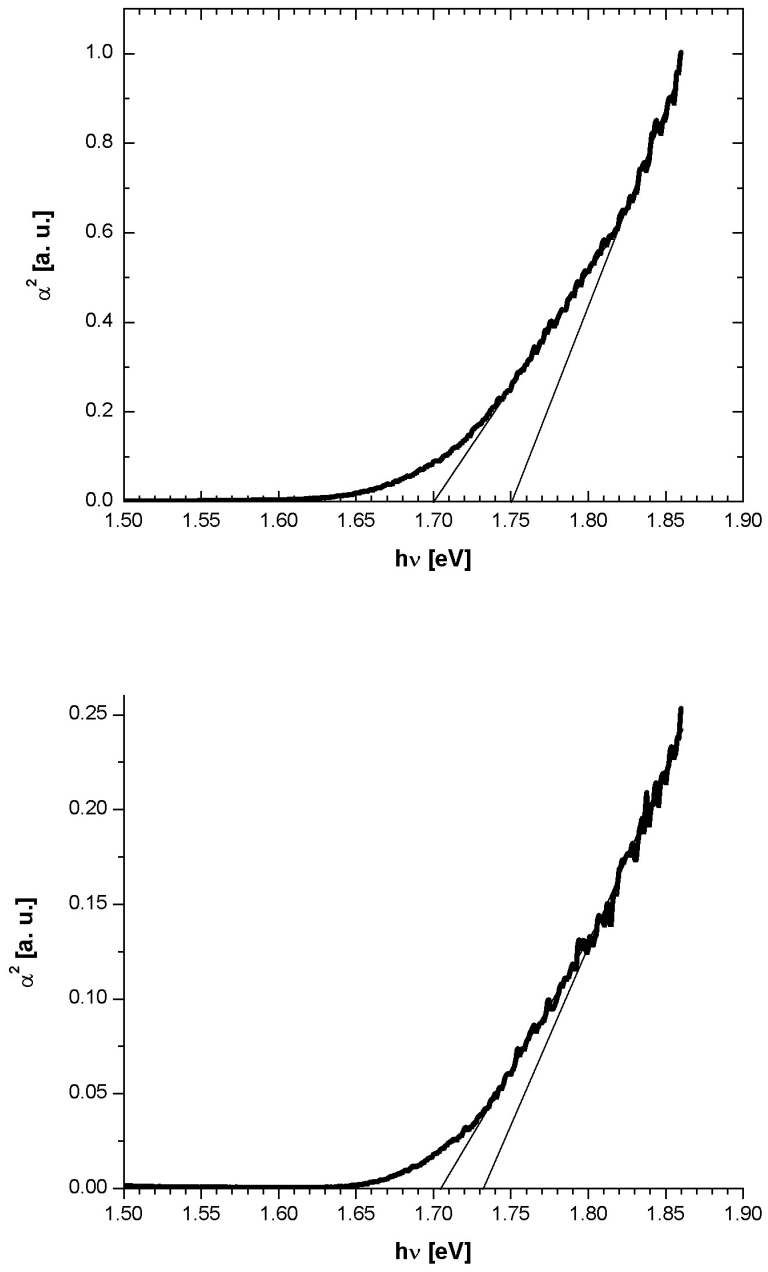

Figure 3.3: α^2 spectra of CdSe 3/24/03 (top) and CdSe 3/28/03 (bottom). Extrapolation lines intersect the $h\nu$-axis at the energy gap according to Equation 3.26.

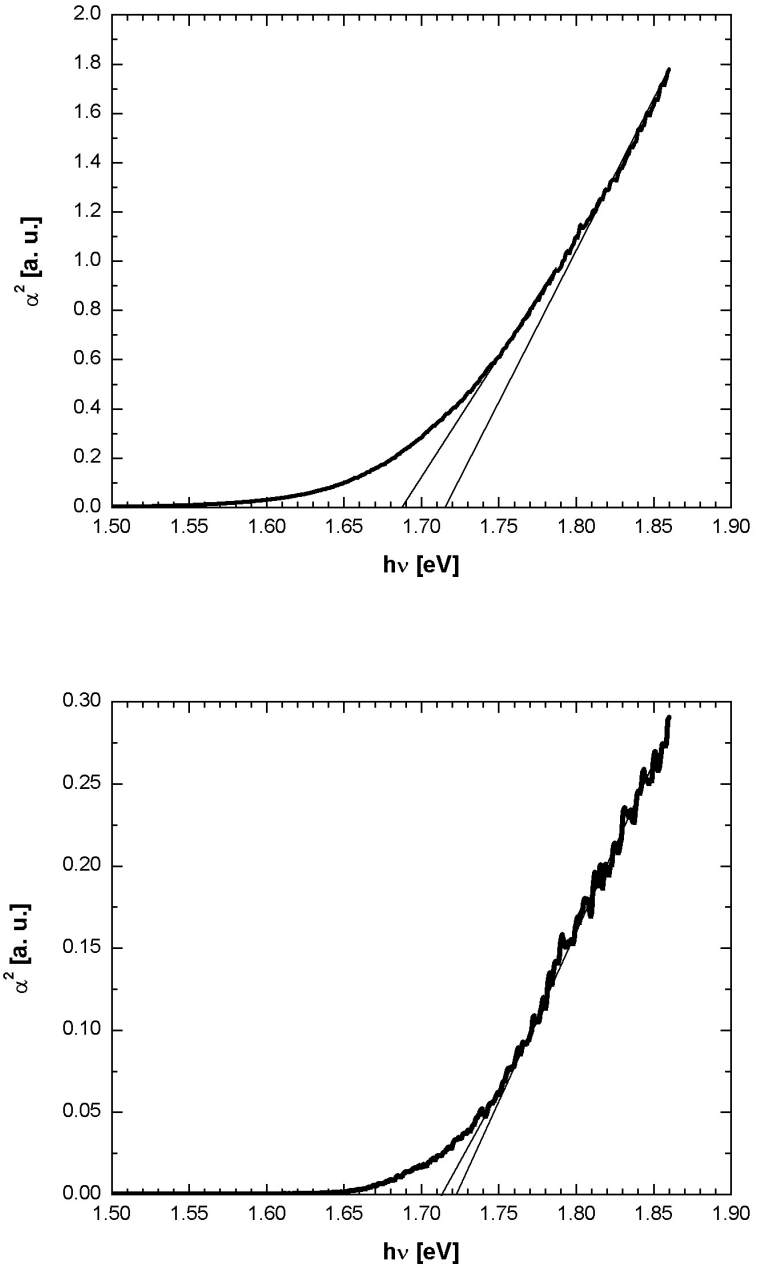

Figure 3.4: α^2 spectra of CdSe 3/30/03 (top) and CdSe 3/31/03 (bottom). Extrapolation lines intersect the $h\nu$-axis at the energy gap according to Equation 3.26.

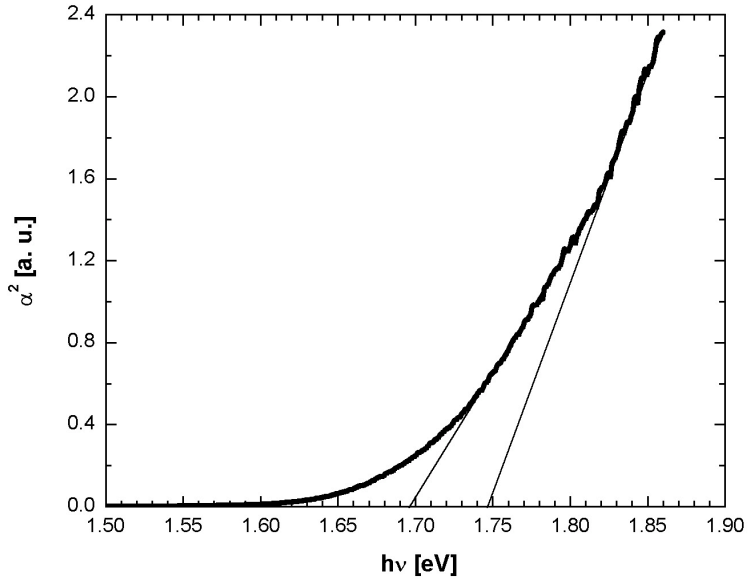

Figure 3.5: α^2 spectrum of CdSe 3/28/03-2. Extrapolation lines intersect the $h\nu$-axis at the energy gap according to Equation 3.26.

Table 3.2: PbSe thin films grown using the method of EC-ALE. The deposition potentials were determined from cyclic voltammograms reported in Chapter 2. The deposition potential was ramped according to Equation 2.2 for the first ten cycles of each film.

Sample	**Cycles**	**Deposition Potentials [V]**
PbSe 5/20/03	85	Pb & Se: $-0.200 \rightarrow -0.270$
PbSe 5/17/03	50	Pb & Se: $-0.200 \rightarrow -0.270$
PbSe 6/11/03	30	Pb & Se: $-0.200 \rightarrow -0.300$
PbSe 6/11/03-1	25	Pb & Se: $-0.200 \rightarrow -0.300$
PbSe 6/11/03-2	20	Pb & Se: $-0.200 \rightarrow -0.300$
PbSe 6/11/03-3	15	Pb & Se: $-0.200 \rightarrow -0.300$
PbSe 6/11/03-4	10	Pb & Se: $-0.200 \rightarrow -0.300$

3.3.3 PbSe

PbSe is a IV-VI compound semiconductor that exhibits rock salt crystal structure with a face-centered cubic (fcc) space lattice. Its lattice constant, $a = 6.124$ Å is the distance along the unit cube edge between two Pb ions. The body diagonal of the unit cube between two Pb ions is $a\sqrt{3}$. The positions of the Pb and Se ions in the unit cell are:

$$\text{Pb} : (0,0,0); (\frac{a}{2}, \frac{a}{2}, 0); (\frac{a}{2}, 0, \frac{a}{2}); (0, \frac{a}{2}, \frac{a}{2})$$

$$\text{Se} : (\frac{a}{2}, \frac{a}{2}, \frac{a}{2}); (0,0, \frac{a}{2}); (0, \frac{a}{2}, 0); (\frac{a}{2}, 0, 0)$$

The Brilliouin zone of PbSe is typical of a fcc latice with symmetry points Γ, L, and X. The Γ point is located at the center of the Brillouin zone with eight L points at the centers of hexagonal faces perpendicular to the [111] direction. Six X points are located at the centers of square faces perpendicular to the [001] direction [7].

Table 3.3: Literature values [7,8] of PbSe's effective electron and hole masses (m_e^* and m_h^*, respectively), effective reduced mass (μ), and the isotropic average effective mass (m^*).

Ref.	m_e^*/m_e	m_h^*/m_e	μ/m_e	m^*/m_e
7	0.050	0.045	0.022	0.048
8	0.084	0.070	0.038	0.077

PbSe has eight surfaces of constant energy ($dE/dk = 0$), one for each of the valence and conduction bands. The constant energy sufaces take the shape of prolate ellipsoids of revolution and center at the L points with major axes in the [111] directions. The valence band maximum and conduction band minimum both occur at the L points, therefore exhibiting a direct fundamental energy gap of .15 eV at ∼0 K and 0.28 eV at 300 K [8]. Unusually, PbSe exhibits a positive temperature coefficient dE_g/dT between 80 K and 373 K. Like most narrow-gap semiconductors, PbSe has a relatively large dielectric constant, $\epsilon_\infty = 23$ [8], and small effective electron and hole masses, m_e^* and m_h^*, all of which are responsible for its large exciton Bohr radius (Chapter 1). There are discrepancies in the effective masses of PbSe reported by Dalven [7] and Kang *et al.* [8], and they are listed in Table 3.3.

Globus *et al.* [9] and Dalven [7] have reported absorption data of PbSe showing absorption coefficients on the order of 10^4 cm^{-1} near the absorption edge. However, measurements of α reported for this thesis show values on the order of 10^5 cm^{-1}, which correspond to a measured I/I_o ratio of ∼ 0.1 (Fig. 3.6). Using Equation 3.18, a transmittance value, I/I_o, of ∼ 0.9 should be expected when measuring the absorption coefficient of a film of ∼70 nm thickness (100 cycles), which corresponds to a value of α that is on the order of 10^4 cm^{-1}. Essentially, the absorption signal

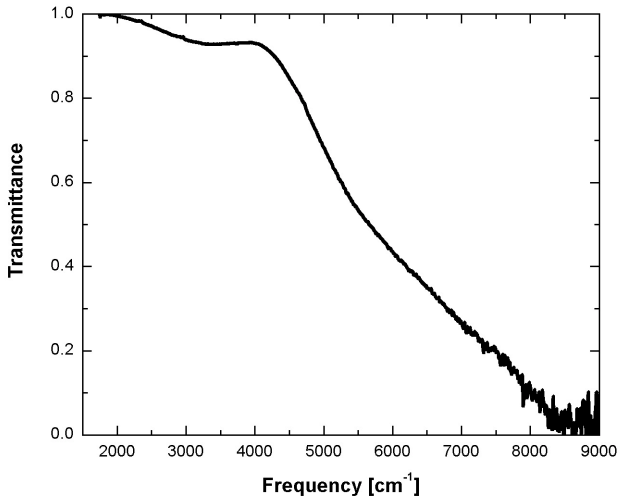

Figure 3.6: Transmittance plot of PbSe 5/20/03 (85 cycles). The film exhibits nearly 100% absorption of incident radiation.

measuring the fundamental energy gap transition of a PbSe thin film is so weak that it is nearly unidentifiable from optical absorption measurements. A clear absorption edge relating to the fundamental energy gap transition is shrouded by phonon transitions, which are manifested in what is known as an Urbach tail of an absorption spectrum [6,9] (Fig. 3.7).

Globus *et al.* [9] were challenged by measuring the energy gap of PbSe, but use the subtle details of the the measured absorption coefficient to successfully find a value $E_{\mathrm{g}} = 0.290 \pm 0.002\,\mathrm{eV}$ at 310 K. This value agrees well with the literature values of the energy gap of PbSe [7,8]. The absorption edge of the direct energy gap of PbSe may be obscured by higher order transitions, but the value of the fundamental direct energy gap of PbSe coincides with the position of the first significant peak in a spectral plot of the derivative of the absorption coefficient with respect to photon

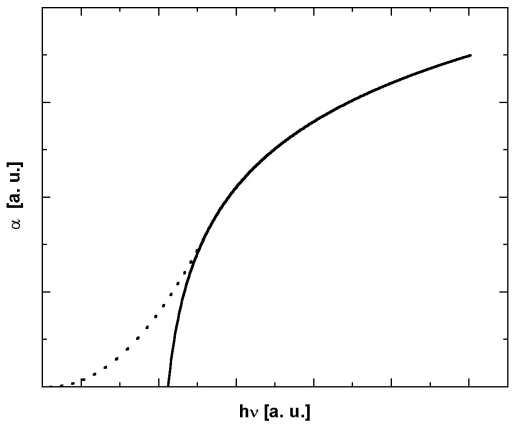

Figure 3.7: Graphic reasoning for using the spectra of $d\alpha/d(h\nu)$ to determine the energy gap of PbSe. The solid line represents an idealized absorption edge that is free of phonon induced transition effects, which are manifest in an Urbach tail (dotted line) near $\alpha = 0$ [6]. The energy gap coincides with the energy of the solid line where $\alpha = 0$. The derivative of an absorption spectrum augmented by an Urbach tail would reveal a peak near the energy gap.

energy. Illustrated in Figure 3.7, the reasoning behind this method is based on what an idealized absorption spectrum PbSe would look like if it were measured at absolute zero temperature. In this case, phonon induced transitions would be diminished, and the value of the energy gap can be determined to be the energy at which $\alpha = 0$. Given an absorption spectrum that is augmented by an Urbach tail, it follows that the spectrum of the derivative of α with respect to $h\nu$ would exhibit a peak near the true energy gap value. As a caveat, Globus *et al.* [9] concede that the identification of these energy gap peaks is ambiguous and should be replaced with a more reliable method.

Using data from transmittance measurements obtained from FTIR spectroscopy, plots of $d\alpha/d(h\nu)$ *vs.* $h\nu$ were calculated for PbSe films grown by EC-ALE. Absorption coefficient values were calculated from raw data and fit to a 9^{th} order polynomial. The fit polynomial divided by the raw data exhibits a generally constant relation with energy, which credits the validity of the computer fit line. Derivatives of the computer fit data were plotted, and extrema were readily decipherable in the energy spectra like that shown in Figure 3.8. The compiled data are listed in Table 3.4.

Figures 3.9 (top) and 3.10 (top) show the energy gap data of the PbSe films listed in Table 3.4 compared to the energy gap dependence on film thickness using the effective mass approximation of Equation 3.15. The reduced mass, μ, was calculated using the values listed in Table 3.3 provided by Dalven [7] (dotted line) and Kang *et al.* [8] (solid line). The data are also compared to the confinement model devised by Wang *et al.* [4], which is referred to as the hyperbolic band approximation, in Figures 3.9 (bottom) and 3.10 (bottom). To calculate the energy gap as a function of film thickness for this model, the average isotropic masses, m^* (Table 3.3), are calculated from the effective mass values reported by both Dalven [7] (dotted line) and Kang *et al.* [8] (solid line).

The PbSe thin films listed in Table 3.2 are not formed by full "monolayers" of the semiconductor compound, which is evident from coverage calculations described in Section 2.4. These calculations represent the fraction of the substrate surface area that is covered by a layer of ions for each cycle of the deposition process. To better estimate each PbSe film's thickness, the average coverage factor (Table 3.4) of each film is multiplied by its theoretical thickness assuming that the film grows in the [111] direction of the PbSe Bravais lattice. Using these alternate values of film thickness, the energy gap data were plotted again in Figure 3.10, and the data appear to agree better with the hyperbolic band model. The literature suggests that

Table 3.4: PbSe energy gap deduced from peaks in each film's spectrum of the derivative of the absorption coefficient with respect to energy. Theoretical film thickness (t_{Th}) values are calculated from the assumption that the PbSe films grow in the [111] direction with a lattice constant of 6.124 Å. The alternative film thickness values (t_{C}) are calculated by multiplying the theoretical film thickness by the coverage factor. An X signifies that there the coverage factor could not be determined.

Cycles	E_{g} **[eV]**	t_{Th} **[nm]**	**Coverage Factor**	t_{c}
85	0.329 0.312	30.05	0.75	23
50	0.485 0.446 0.424	17.68	X	X
30	0.532 0.532 0.527	10.61	0.91	9.7
25	0.350 0.306	8.393	0.73	6.1
20	0.811 0.715	7.071	0.79	5.6
15	0.752 0.560 0.548	5.304	0.78	4.1
10	1.214 1.156 1.119	3.395	0.96	3.4

quantum confined PbSe is modeled well by the hyperbolic band model for dimensions greater than several Angstroms [4,8].

Uncertainties in the data points are mainly caused by inaccurate thickness estimations of the thin films. Also, the surface character of the films may affect the measured electronic properties of the these semiconductor films, which will be discussed in Section 3.4.

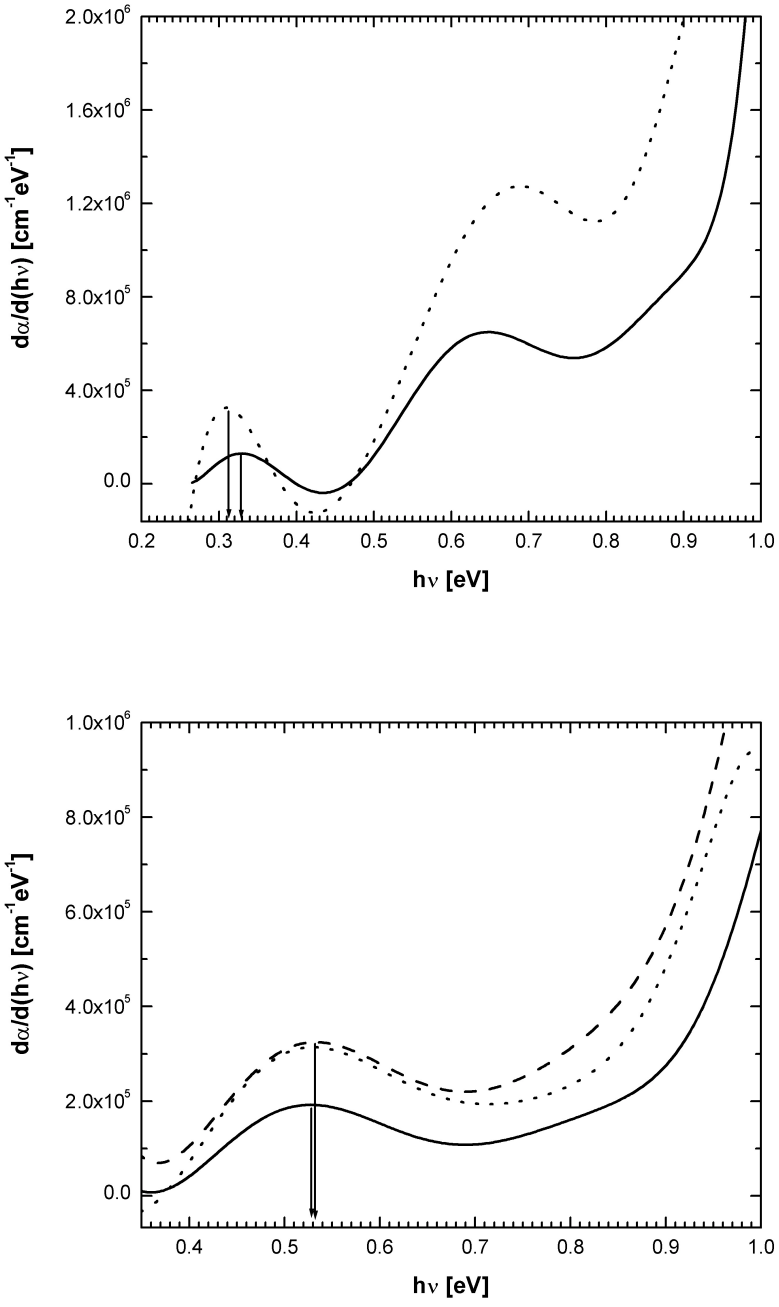

Figure 3.8: Energy gap values of PbSe thin films were determined from the first significant peak in the energy spectra of $d\alpha/d(h\nu)$. Top: PbSe 5/20/03, 85 cycles. Bottom: PbSe 6/11/03, 30 cycles. Tables 3.2 and 3.4 report the energy gap values determined using this method for all PbSe samples in this study.

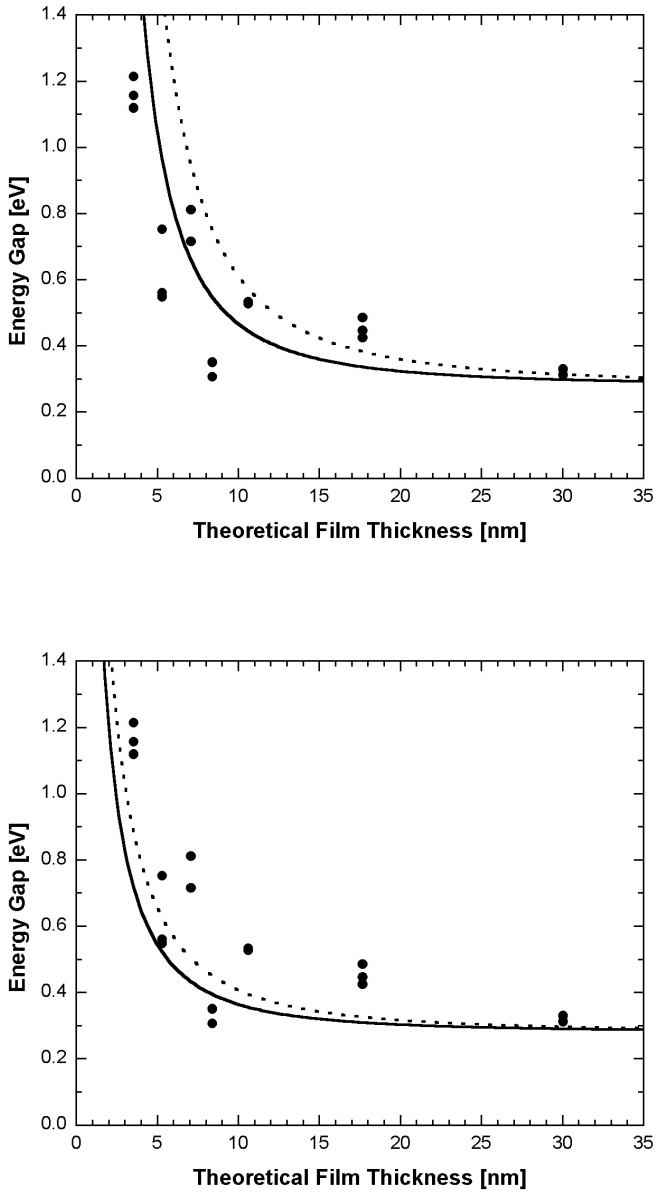

Figure 3.9: Energy gap values of PbSe thin films were determined from plots of $d\alpha/d(h\nu)$ [9] and are shown to exhibit quantum confinement effects. The values for energy gap were plotted with respect to theoretical film thickness and compared to the predictions of two different theoretical models. Top: Effective mass approximation [4]. Bottom: Hyperbolic band model [4]. Solid Line: Effective mass values of Ref. 8. Dotted line: Effective mass values of Ref. 7.

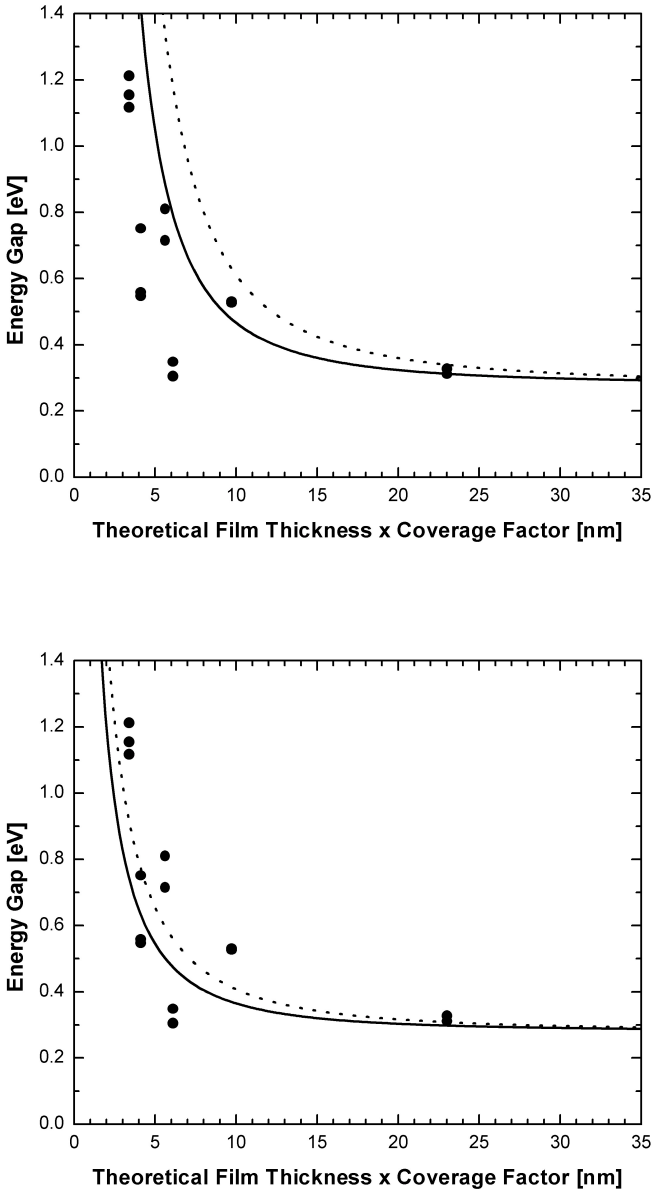

Figure 3.10: Energy gap values of PbSe thin films were determined from plots of $d\alpha/d(h\nu)$ [9] and are shown to exhibit quantum confinement effects. The values for energy gap were plotted with respect to theoretical film thickness $\times$ the average coverage factor for each film and compared to the predictions of two different theoretical models. Top: Effective mass approximation [4]. Bottom: Hyperbolic band model [4]. Solid Line: Effective mass values of Ref. 8. Dotted line: Effective mass values of Ref. 7.

3.4 Morphology

The quality of a thin film semiconductor is reflected in its surface morphology, and surface images on a nanoscopic scale can reveal growth patterns of the semiconductor films. A correlation between the electronic properties and the surface morphology of the EC-ALE semiconductor thin films is explored in this thesis, which is exhibited in samples of CdSe films. Also, the films' epitaxial character may be judged by growth characteristics evident from nanoscopic surface features. To analyze the growth characteristics of EC-ALE films, images of a bare Au substrate are compared to the images of the semiconductor depositied on the substrate, where ideal epitaxial semiconductor growth is apparent if the deposited semiconductor reflects the substrate surface character. The surfaces of EC-ALE thin films reported in this thesis were probed with an atomic force microscope, however a scanning electron microscope or a scanning tunneling microscope could be used to yield the same results.

3.4.1 Atomic Force Microscopy

The atomic force microscope (AFM) (Dimension^{TM} 3100 Nanoscope, Digital Instruments, Veeco Metrology Group, Woodbury, NY) is a device used to measure nanometer-sized surface features. Unlike a light microscope, the AFM uses a cantilever tipped with a Si crystal to probe a surface. A clear 1×1 micron image captured with an AFM can resolve lateral features with 1.95 nm resolution, which clearly gives an advantage over light microscopes. However, unwanted errors caused by the crystal tip shape and drift are possible and sometimes inescapable (Figure 3.11) [10].

The AFM images a surface by detecting the deflection of a low-wattage diode laser that is reflecting off of the probe cantilever. There are two standard modes

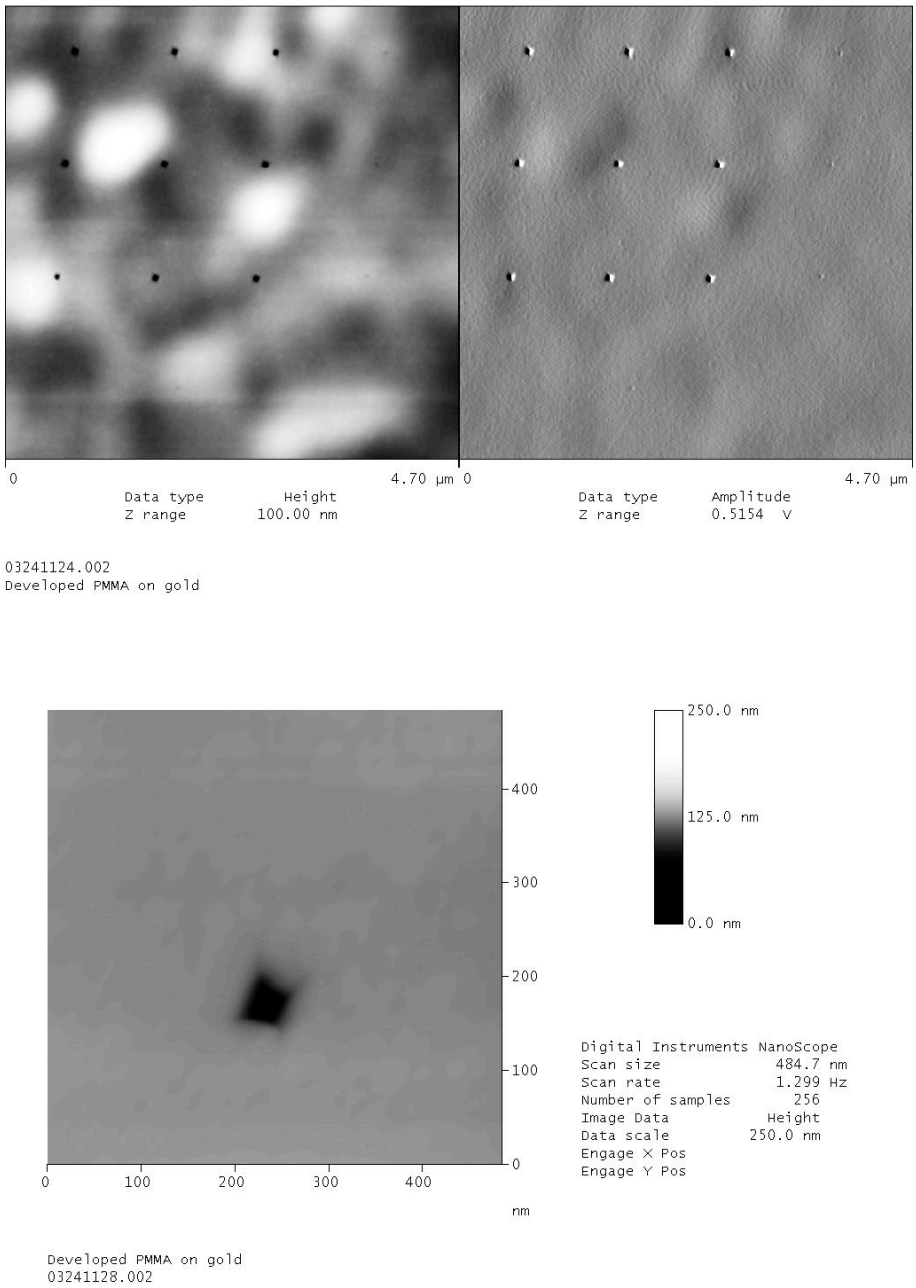

Figure 3.11: AFM image of an array of circles in PMMA-coated Si substrate created by Nanometer Pattern Generation System in conjuction with the SEM (Left: Topographical; Right: Tip amplitude). Bottom: Topographical image of 50 nm wide hole that is barely visible right area of the in the top figure. Clearly, the pyramidal shape of the Si AFM tip is imaged rather than the true shape of the hole.

of operation for the AFM that are referred to as *contact* and *tapping*. In contact mode, the probe is dragged across the sample surface, where surface features cause the cantilever to bend accordingly. The AFM tries to keep the probe at a constant distance from the sample surface at all times and compensates for the cantilever bending using a piezo element that reacts to feedback from the diode laser deflection detector. The z-direction of the piezo correction movements are plotted by the AFM's computer as a function of lateral probe position to make a square topographical image of a surface. In tapping mode, the cantilever is made to vibrate near its resonant frequency (10^2 kHz) while imaging a surface. The reflected diode laser is detected as a sinusoidal signal. As the probe is moved across a sample surface, its features will cause the amplitude of the vibrating cantilever to change. The AFM feedback circuit tries to keep the amplitude constant, thus keeping tip-sample separation constant, and compensates for surface height changes with the piezo element. Again, topographical images of a sample surface can be imaged by plotting the z-direction movement of the piezo element as a function of lateral distance. The change in the cantilever's vibration amplitude can also be plotted as a function of lateral distance, essentially giving an image of derivative of the height data with respect to lateral distance [10]. In this thesis, the AFM's tapping mode was used exclusively using a Si tipped cantilever, and both topographical and tip amplitude plots are included in most AFM figures in this thesis. Also, all imaging was performed in ambient air at room temperature.

Primarily, AFM was used to study the growth characteristics of the thin films. The Au substrate and semiconductor surface of each sample were imaged and compared. Epitaxial growth would be apparent if the Au substrate's features are reflected in the features of the semiconductor. AFM images defining non-epitaxial growth do not resemble the substrate surface and often resemble form of "cauliflower" in a $5 \times 5\,\mu$m scan as shown in Figure. 3.12.

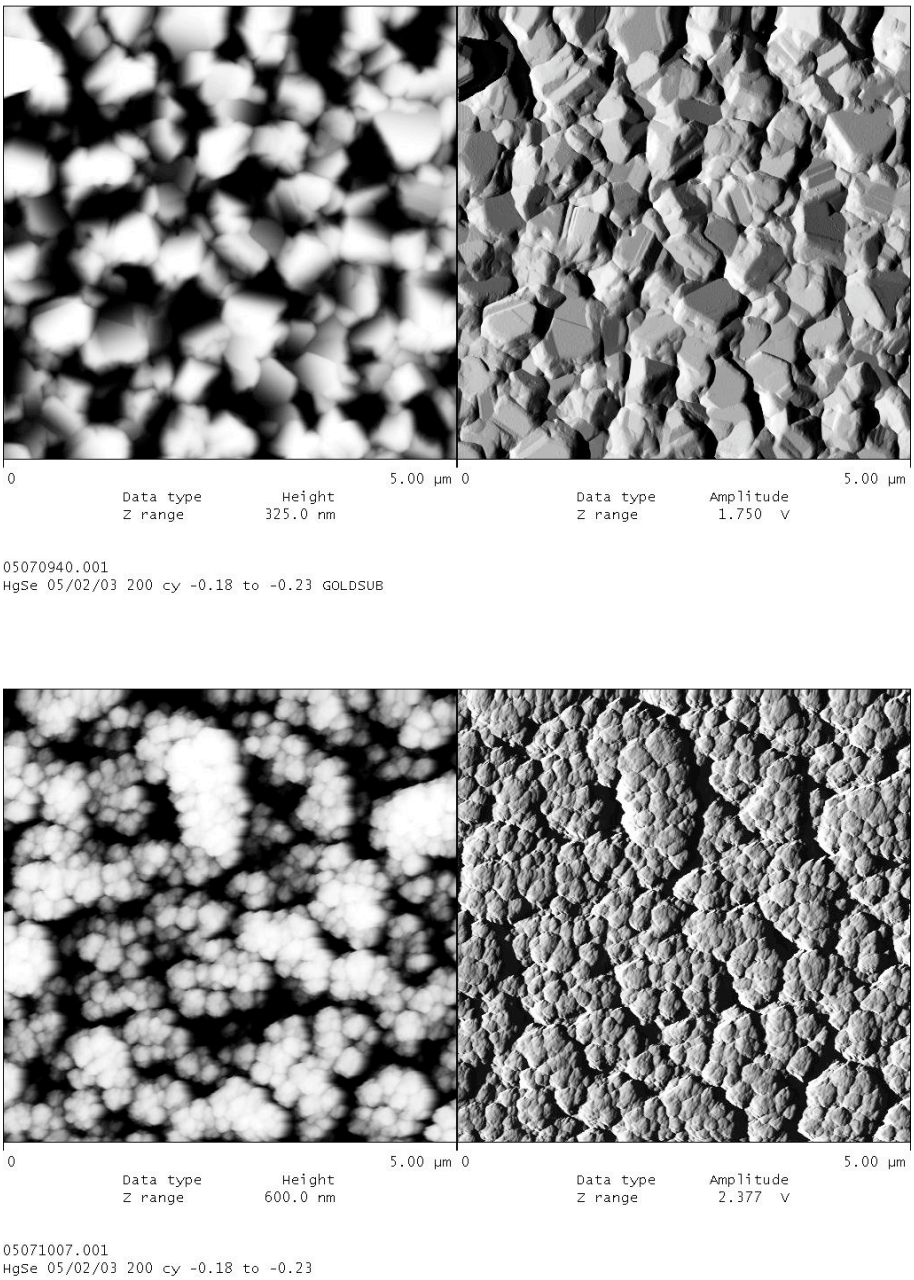

Figure 3.12: An example of nonepitaxial semiconductor growth. The top image shows the Au substrate, and the bottom image shows a semiconductor film (HgSe 5/02/03). The semiconductor sample does not reflect the surface of the Au substrate, and is therefore a non-epitaxial formation.

Au substrates that macroscopically appeared to have a dull shine with a pinkish tint exhibited well-defined 200–600 nm diameter plateaus when imaged with the AFM (Fig. 3.12, *top*), while Au substrates appearing with the familiar gold color and shiny appearance exhibited a melted, sand-dune appearance in a 5×5 micron image (Fig. 3.14, *top*). Most Au substrates appeared to exhibit surface features with less defined, yet observable plateau structures with flat regions oriented at widely varying angles from parallel to the glass slide.

3.4.2 CdSe

$5 \times 5\,\mu$m images of each CdSe sample were compared to each sample's respective Au substrate. The varying features of each sample's Au substrate and growth patterns are clearly noticeable from the AFM images. Figure 3.13 shows the terraced character of the Au substrate of sample CdSe 3/06/03 (200 cycles), which appears lightly powdered over the sharp Au features. Figure 3.14 exhibits the completely unterraced and soft features of the Au substrate of the sample CdSe 3/28/03-1 (200 cycles), and the semiconductor surface appears powdered but with larger particle grains than that of CdSe 3/06/03, as is the case with the remaining CdSe samples. Listed in Table 3.1, samples with undeterminable energy gaps also exhibited sample growth that was immeasurable by the AFM signifying that the surface features of those samples exceeded several microns in height. The fact that the measured band gap of CdSe 3/06/03 (Table 3.1) matches the literature value of 1.74 eV for CdSe at room temperature [6], while the others did not, indicates that this semiconductor film's growth characteristics affect the electronic quality of the deposited semiconductor.

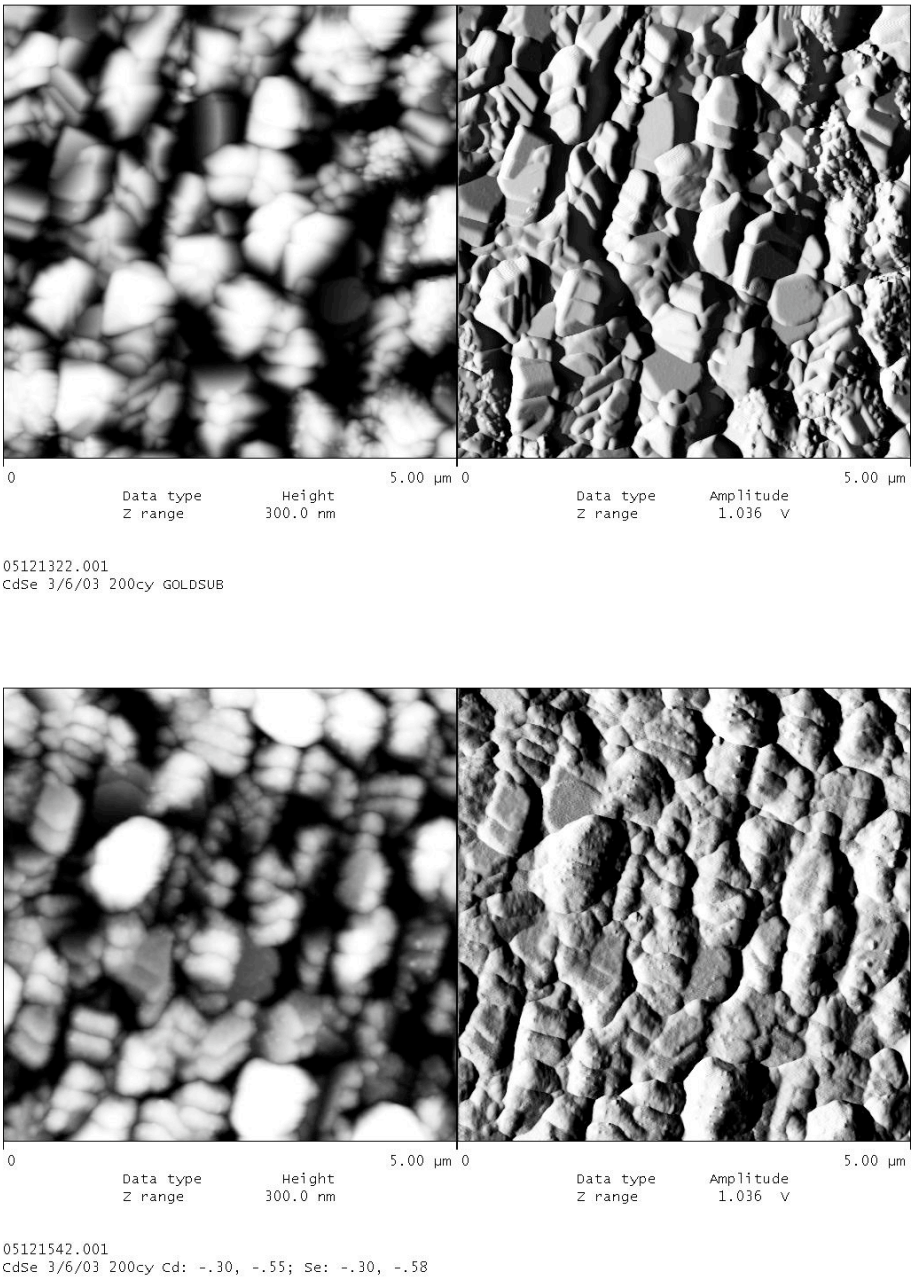

Figure 3.13: AFM images of CdSe sample 3/6/03 (200 cycles). Top is an image of the Au substrate. Bottom image is the sample surface. Here, the terraced features of the Au substrate and the growth pattern of the CdSe film are clearly visible as a light powdering on the substrate (Left: Topographical; Right: Tip amplitude).

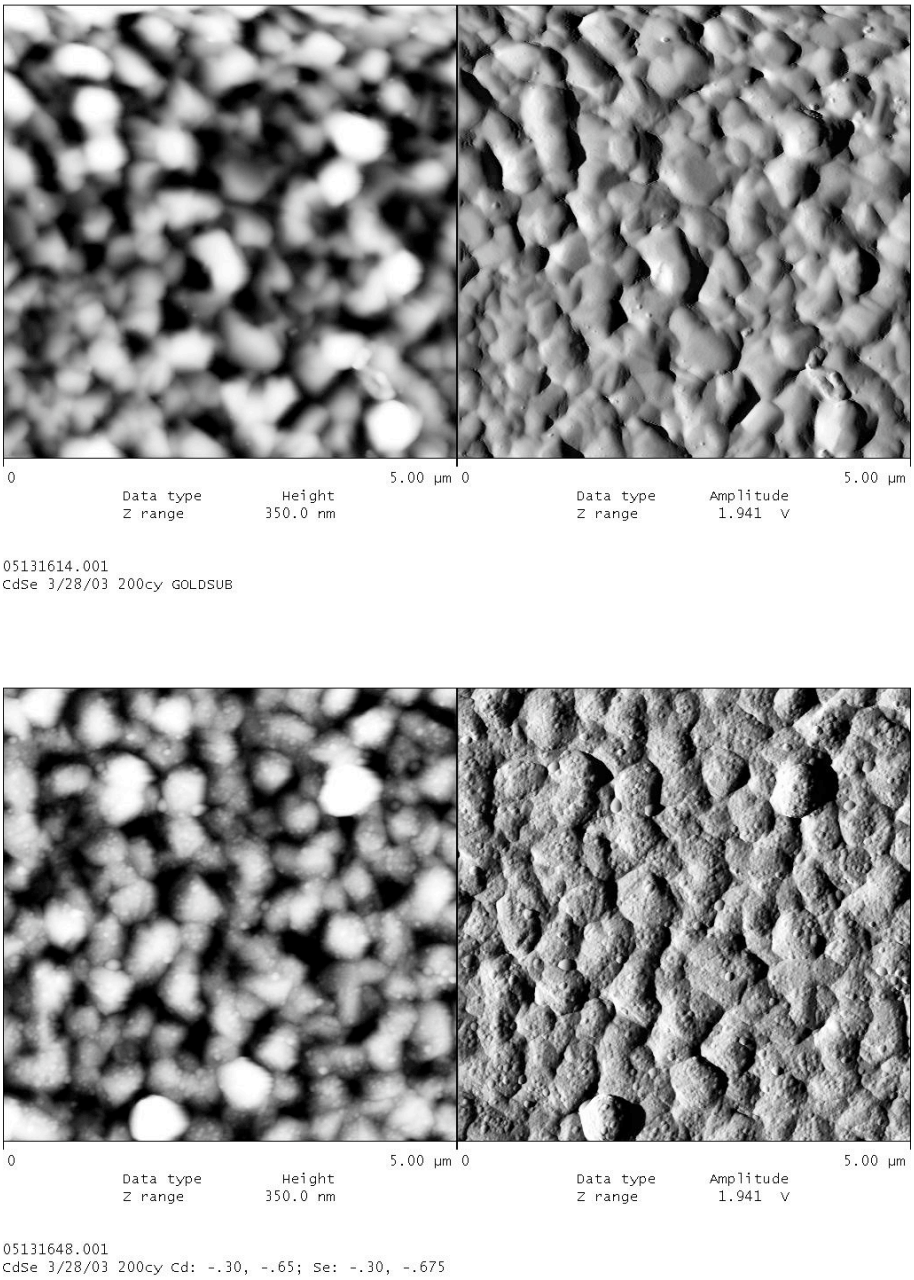

Figure 3.14: AFM images of CdSe sample 3/28/03 (200 cycles). Top image is the Au substrate. Bottom image is the sample surface. The Au substrate exhibits no terracing, and the sample growth contains more particle formation than that exhibited by CdSe 3/06/03 in Figure 3.11 (Left: Topographical; Right: Tip amplitude).

3.4.3 PbSe

PbSe samples were also imaged with the AFM and 5 x 5 micron images were compared. Figure 3.15 shows the Au substrate (top) and semiconductor surface (bottom) of PbSe sample 6/11/03-4; 10 cycles, which exhibits a semiconductor surface of relatively low particle density. Similarly, PbSe 6/11/03-3 (15 cycles) and 6/11/03-2 (20 cycles) (Fig. 3.16) both display surface characteristics favoring epitaxial growth. However, the remaining PbSe thin films studied in Table 3.2 exhibit a high particle density ($> 50\,\text{nm}$) on each semiconductor surface (Figs. 3.17, 3.18), the 50 cycle sample being the most dramatic. These imperfect samples are not characteristic of epitaxy, and their three dimensional growth may also cause deviations in their expected electronic properties like that seen with the CdSe thin films.

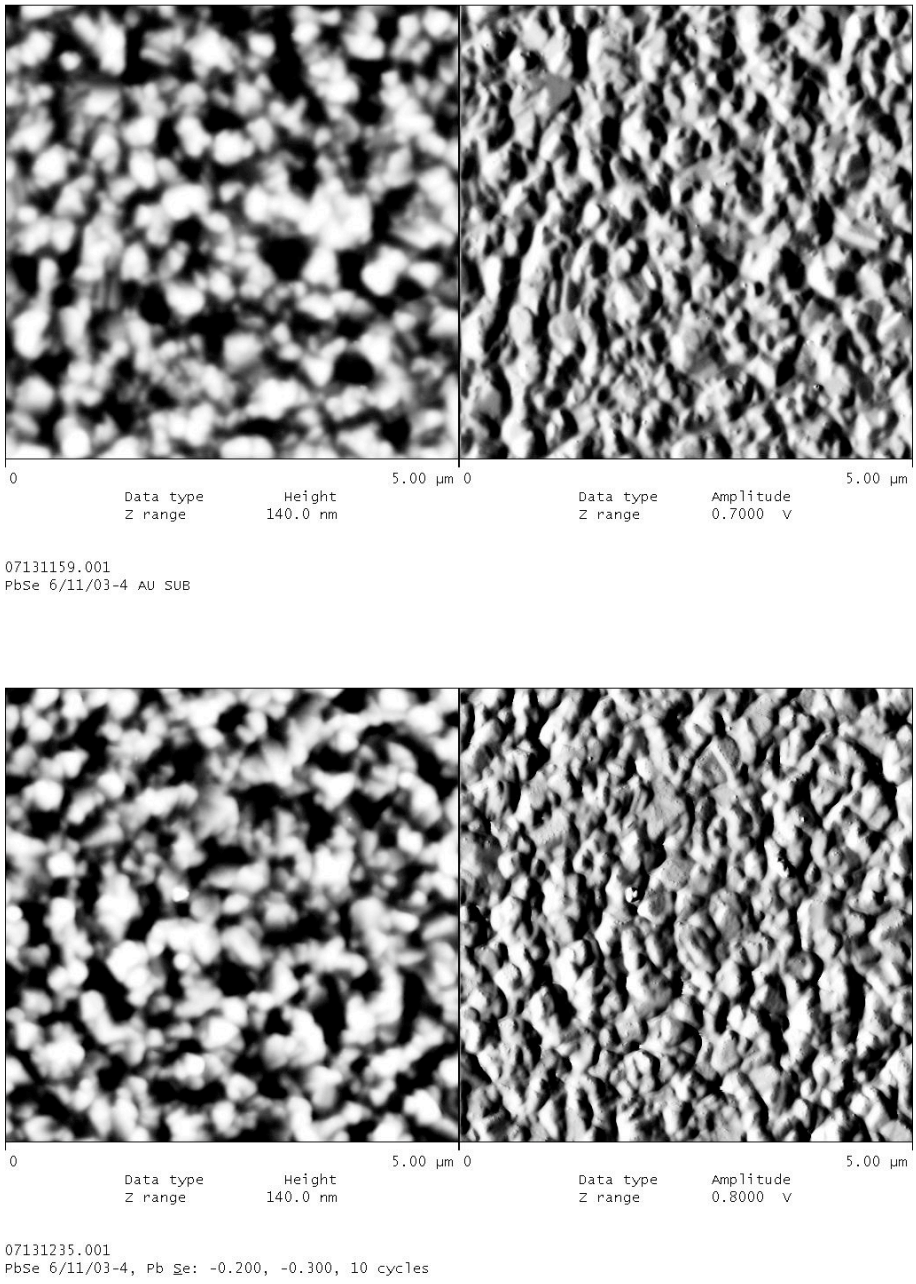

Figure 3.15: AFM images of PbSe sample 6/11/03-4 (10 cycles) (Left: Topographical; Right: Tip amplitude). Top image is the Au substrate. Bottom image is the sample surface.

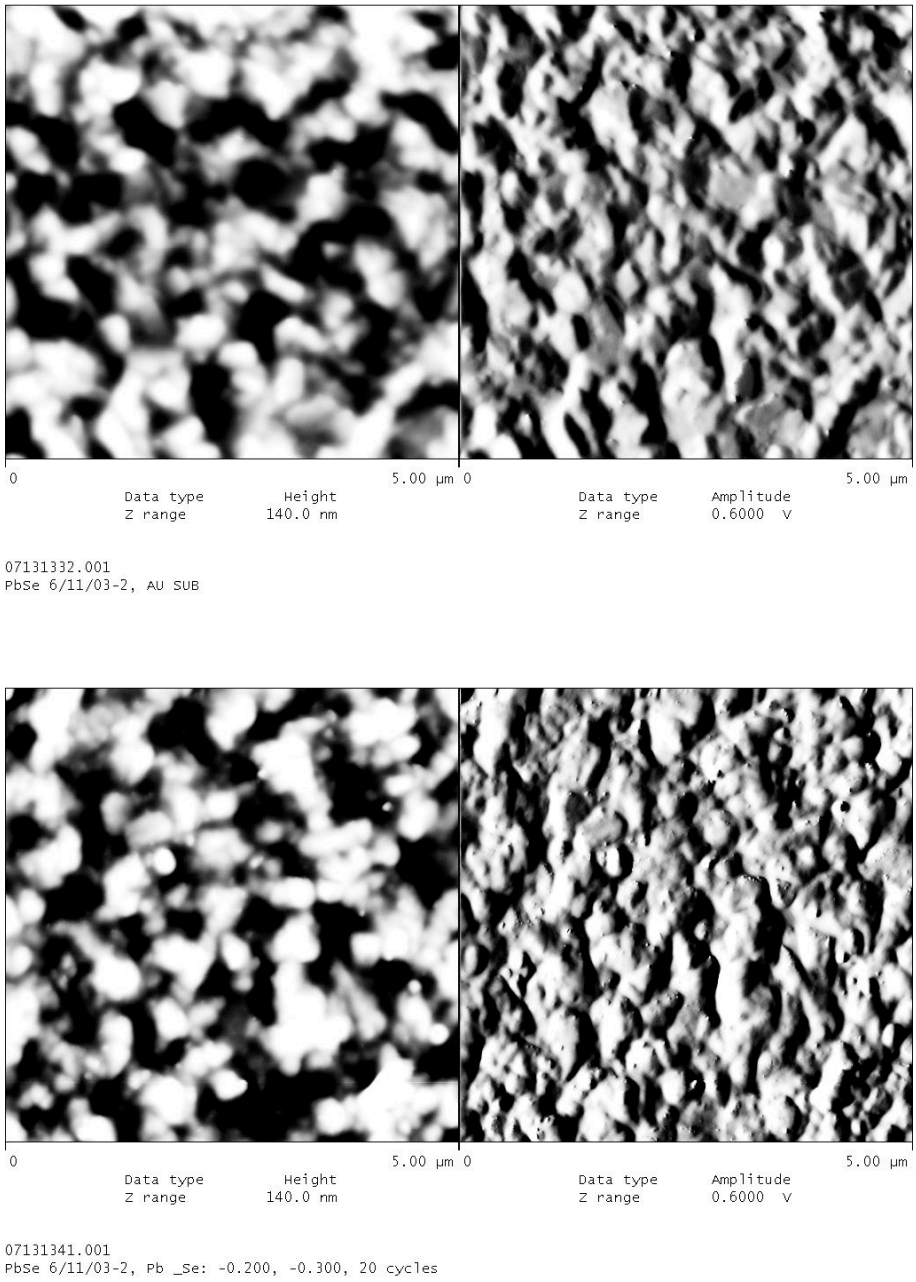

Figure 3.16: AFM images of PbSe sample 6/11/03-2 (20 cycles) (Left: Topographical; Right: Tip amplitude). Top image is the Au substrate. Bottom image is the sample surface.

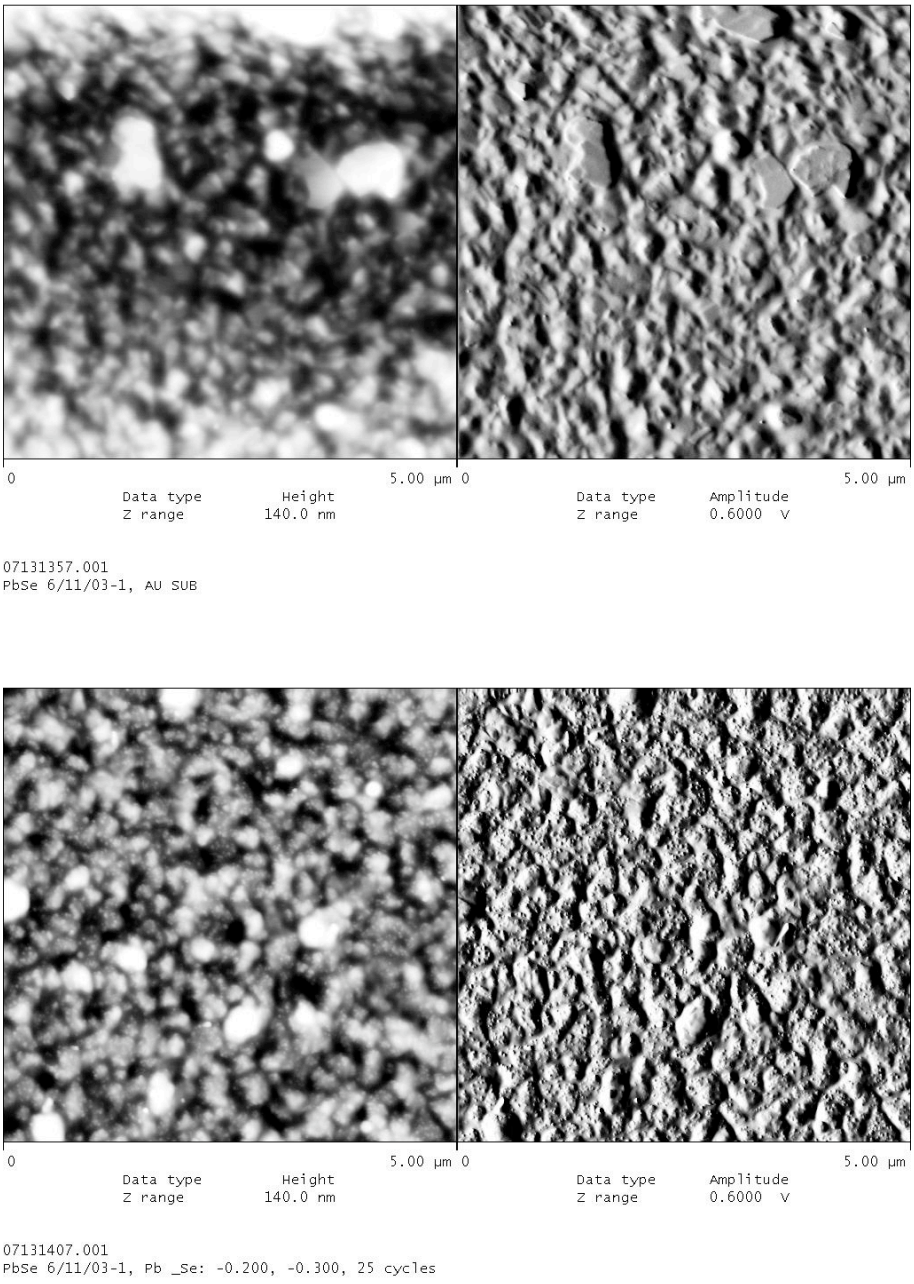

Figure 3.17: AFM images of PbSe sample 6/11/03 (25 cycles) (Left: Topographical; Right: Tip amplitude). Top image is the Au substrate. Bottom image is the sample surface.

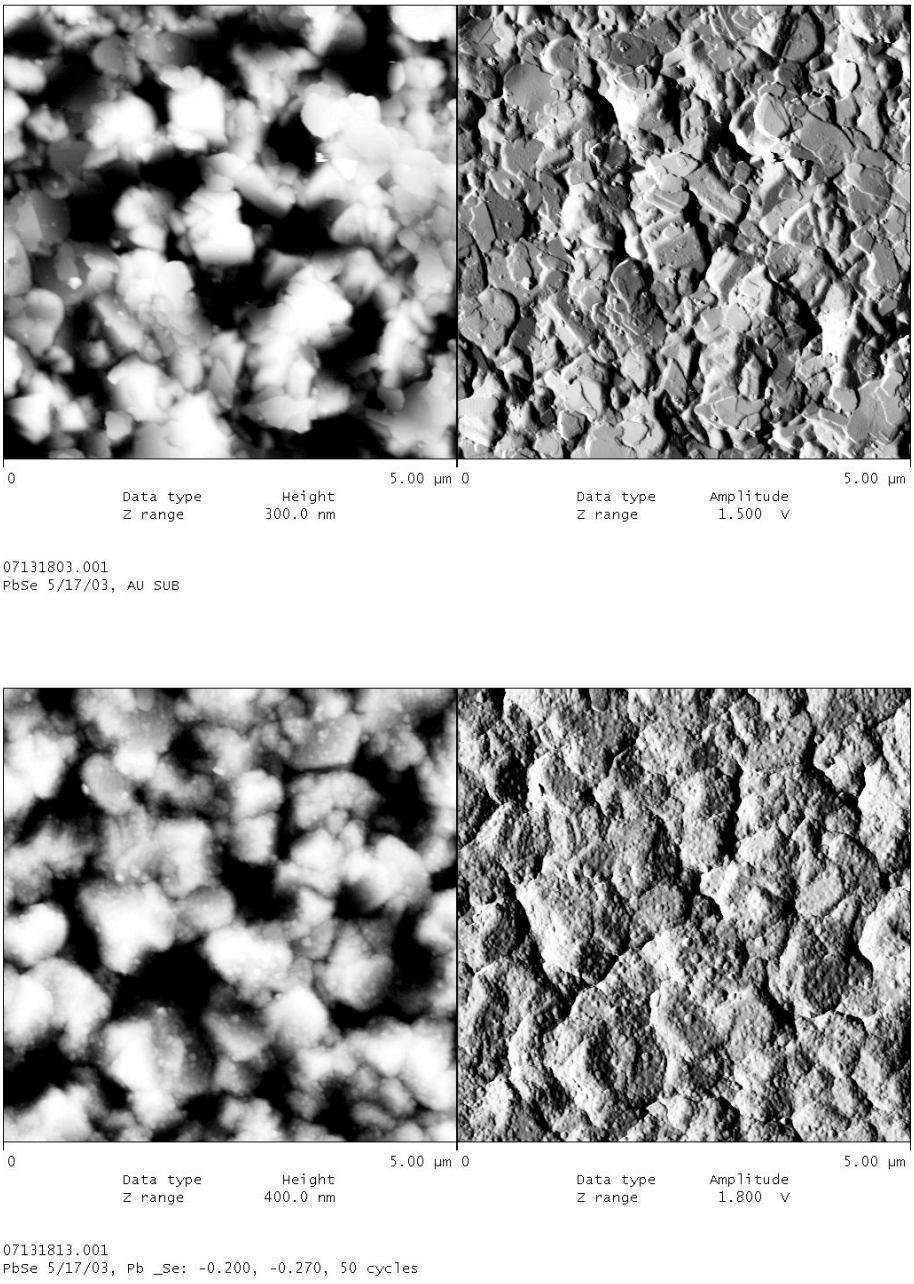

Figure 3.18: AFM images of PbSe sample 5/17/03 (50 cycles) (Left: Topographical; Right: Tip amplitude). Top image is the Au substrate. Bottom image is the sample surface.

3.5 References

[1] M. Fox, *Optical Properties of Solids*, (Oxford University Press, New York, 2001).

[2] J. Singleton, *Band Theory and Electronic Properties of Solids*, (Oxford University Press, New York, 2001).

[3] R. Vaidyanathan, Dissertation, The University of Georgia, 2003.

[4] Y. Wang, A. Suna, W. Mahler and R. Kasowski, J. Chem. Phys., **87**, (1987) 7315.

[5] P. R. Sprinkle, Dissertation, The University of Georgia, 2001.

[6] J. I. Pankove, *Optical Processes in Semiconductors*, (Dover Publications, Inc., New York, 1971).

[7] R. Dalven, Infrared Phys., **9**, (1969) 141.

[8] I. Kang and F. W. Wise, J. Opt. Soc. Am. B, **14** (1997) 1632.

[9] T. R. Globus and A. O. Olesk, Sov. Phys. Semicond., **19**, (1985) 385.

[10] *Dimension*™ *3100 Manual*, *Instruction Manual* (Digital Instruments, Veeco Metrology Group, 2000).

Chapter 4

Conclusion

The observation of size dependent energy gap changes in PbSe thin films formed using the method of electrochemical atomic layer epitaxy can be attributed to quantum confinement effects. As an ensemble, the measured energy gaps of the PbSe thin films are most closely modeled by the hyperbolic band model when plotted with respect to the coverage-corrected values of film thickness. Comparisons of the films' energy gap broadening with respect to the different effective masses that were used in each model is indecisive.

This study of would benefit from explicit measurements of film thicknesses. Also, the semiconductor film deposition methods should be optimized to reduce particle formation, as a correlation between the electronic properties of a semiconductor and its surface morphology has been identified from the study of CdSe. The creation of samples that exhibit positive growth characterics may be reproducible given some procedural optimization.

A future study of quantum confined semiconductor thin films grown using the method of EC-ALE would benefit from more control over each sample's physical size. One way to do this is to localize the semiconductor deposits on a lateral nanometer scale so that film thicknesses could be measured with the precision of an AFM. Structuring the semiconductors on this scale could be done by templating the EC-ALE deposits using electron beam lithography techniques. However, measuring the electronic properties of a nanometer scale semiconductor is impossible using the optical

methods of this study. Therefore, spectroscopy methods using the sub-nanometer capability of a scanning tunneling microscope would be better suited to experiments concerning nanometer scale semiconductors. Both nanolithography and scanning tunneling spectroscopy techniques are currently being employed at The University of Georgia, and they are introduced in the following chapter. The cooperation of these two techniques would be highly effective in measuring quantum confinement effects in future EC-ALE semiconductors.

Chapter 5

Future Study

5.1 Nanolithography

Nanopatterning semiconductor substrate is possible using a Nanometer Pattern Generation System (NPGS) (J. C. Nabity Lithography Systems, Bozeman, MT) and a scanning electron microscope (SEM). NPGS essentially takes control of the SEM's electron beam and writes nanoscale patterns generated with computer aided design software. Currently, NPGS at The University of Georgia is capable of performing lithography consisting of ∼30 nm wide tracks in thin (∼200 nm) layer of poly(methylmethacrylate) (PMMA) resist. Nanopatterns generated by NPGS are only limited by the imagination and the capabilities of the SEM. These tracks can be filled with a semiconductor by some method, and subsequent dissolution of the PMMA template leaves a patterned semiconductor. This method should work as well with EC-ALE and further our work in the nanometer realm [1,2].

Figure 5.1 shows an example of Cr lettering that has been deposited on a Si substrate using NPGS. A spin-coater was used to apply a thin layer of 950k molecular weight PMMA dissolved in chlorobenzene (3% by weight) on a 1 cm^2 wafer of Si. The wafer was initially cleaned in an ultrasonic acetone bath for several hours and dried with N_2. The wafer was further cleaned while spinning, first squirted with acetone, then isopropol alcohol, and spun until dry at 4000 RPM. PMMA solution was applied using a disposable glass pipet as a large single drop that completely covered the Si surface. After the PMMA solution was applied, the wafer was ramped

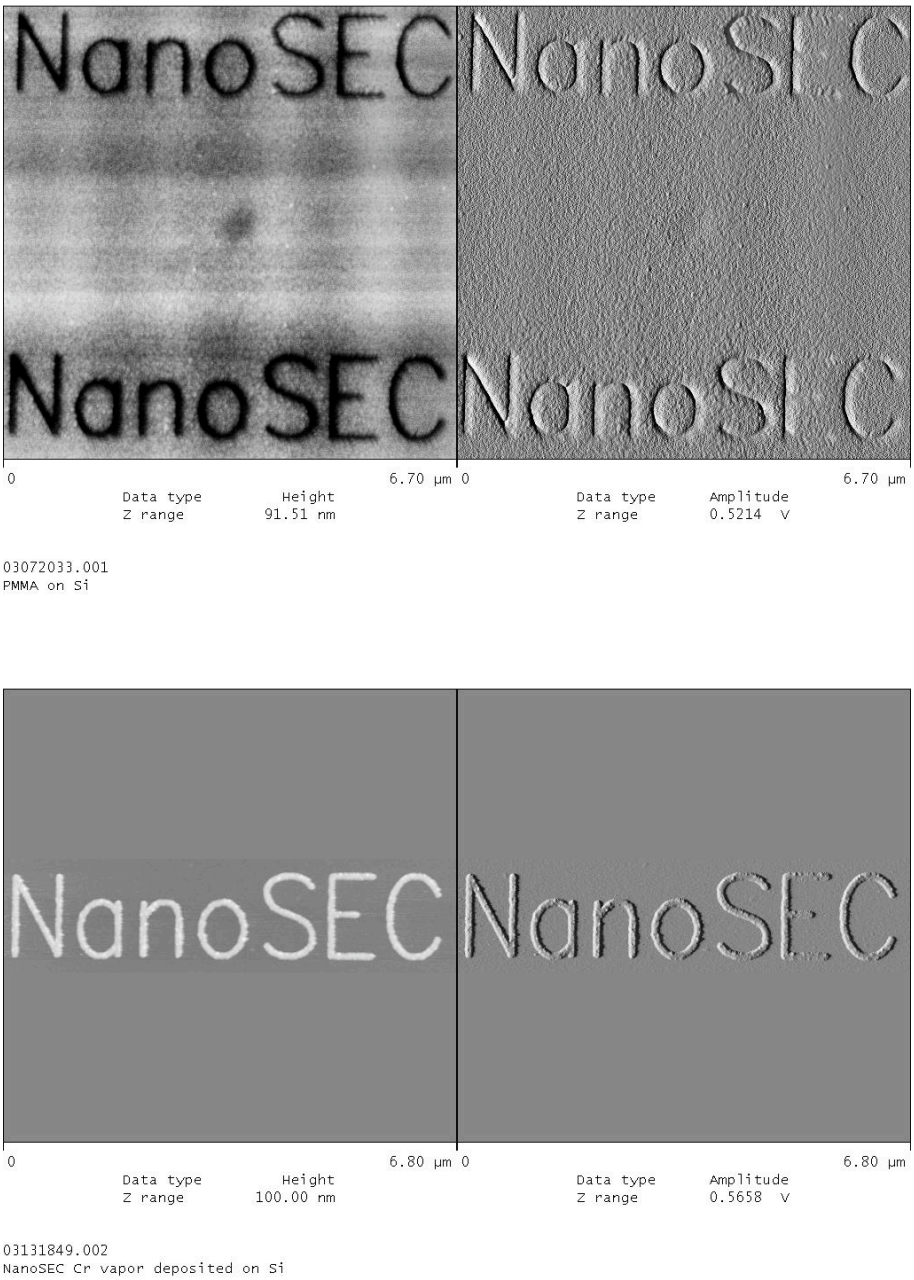

Figure 5.1: Lettering written with NPGS. Top: Topographic (left) and tip amplitude (right) AFM images of lettering written in 180 nm PMMA layer on Si substrate. Bottom: Topographic (left) and tip amplitude (right) AFM images of vapor deposited Cr lettering and no PMMA.

at a rate of 5000 RPM/s to 500 RPM and spun for 5.0 seconds. Then, the spinning wafer was ramped again at a rate of 5000 RPM/s from 500 RPM to 4000 RPM and spun at this speed for 45.0 seconds. The spinning wafer was then braked to a halt at −1000 RPM/s. The first spin speed is needed to spread the resist solution evenly over the substrate surface, and the final spin speed determines the resist's final thickness. The final braking rate appeared to have an influence over the resist's visible quality. No bubbles or visible abnormalities were acceptable on the surface of the PMMA-coated Si wafer before use as a lithographic resist. This entire process was completed in a dark room because PMMA is photosensitive. Although PMMA is less sensitive to UV light used in most laboratories, care was still taken to protect all PMMA resists. Completed resists were protected by wrapping their containers in aluminum foil [2].

Following the initial PMMA spin-coating, the wafer is baked in a convection oven at 160° C for 120 minutes. Omission of the baking step leads to results like that shown in Figure 5.2, where the PMMA is filled with air pockets measuring hundreds of nanometers in diameter which can dramatically decrease the quality of a nanopattern. Also, such air pockets may unfavorably contaminate SEM by outgassing in its evacuated chamber. Even properly baked PMMA samples should be desiccated for at least a day before being placed in the SEM [2].

Patterning the PMMA coated substrate was performed with the electron beam of the SEM (Leo 982 field emission scanning electron microscope, Thornwood, NY) located at UGA's Center for Ultrastructural Research. Patterns for NPGS were made with a computer-aided-design (CAD) program (DesignCAD LT 2000, Upperspace Corp., Pryor, OK). The CAD programs were read by NPGS, which took control of the scanning mechanism of the SEM to write the CAD pattern. The electron beam does not burn patterns into the PMMA, rather it changes the PMMA's molecular character so that PMMA exposed to the electron beam radiation will be soluble in a

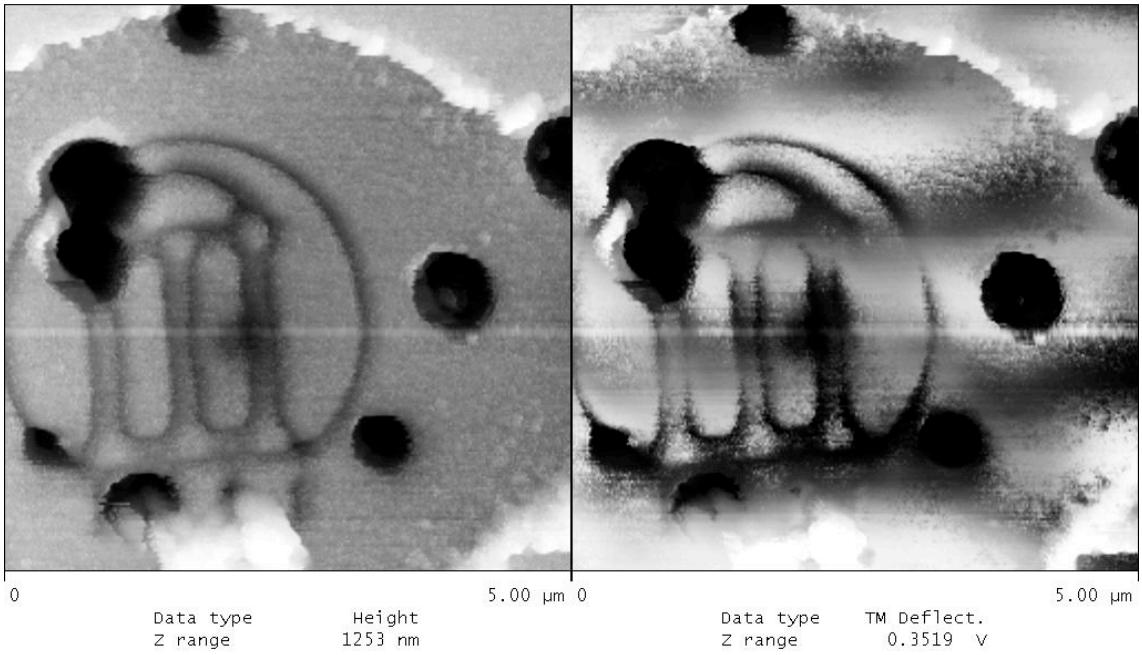

Figure 5.2: Example of the effect of not baking a PMMA coating. UGA arch is speckled by air pockets measuring hundreds of nanometers in diameter (Left: Topographic image; Right: Tip amplitude image).

developer solution, here a 3:1 solution of isopropol alcohol and methyl isobutyl ketone (IPA/MIBK) was used as the developer solution [2]. After exposing the PMMA in the SEM, the PMMA was developed according to the following procedure: The sample was submerged in developer (3:1 IPA/MIBK) for ∼70 s; submerged in pure IPA for ∼20 s; submerged in deionized water for ∼30 s; and dried using nitrogen gas until no moisture was visible on the sample. This essentially carved the pattern out of the PMMA and exposed the Si substrate underneath (Figure 5.1,top).

The patterned PMMA was used to template the deposition Cr onto the Si substrate. The Si wafer was placed in a vapor depositor (Edwards vacuum evaporator, Wilmington, MA) where 8 to 10 nm of Cr was deposited on the wafer. After deposition, the PMMA template was dissolved in an acetone bath inside an ultrasonic cleaner for several hours. The final product was imaged with AFM (Figure 5.1) where the height of the lettering was found to be ∼8 nm.

Patterns are designed in the CAD software to be written multiple times in an array (Figure 5.3). This technique was dubbed the "shotgun" method, which allows the pattern to be written using a range of different electron beam currents. Judging from the array, the exposure parameters of the highest quality pattern can be regarded as optimal. Considering the nanometer dimension of the work created, a large array also makes finding the completed patterns less difficult.

Using this nanopatterning technique, semiconductors with highly controlled dimensions can be grown with EC-ALE. In conjunction with scanning tunneling spectroscopy, localized structures exhibiting three dimensional quantum confinement effects could be studied. At the very least, the object of study could be localized on a nanometer scale, which could allow AFM measurements of region-specific semiconductor structures. Another study of one-dimensional confinement of PbSe grown by EC-ALE could benefit from the ability measure thicknesses with such precision. However, the energy gap of such a localized semiconductor structure cannot be

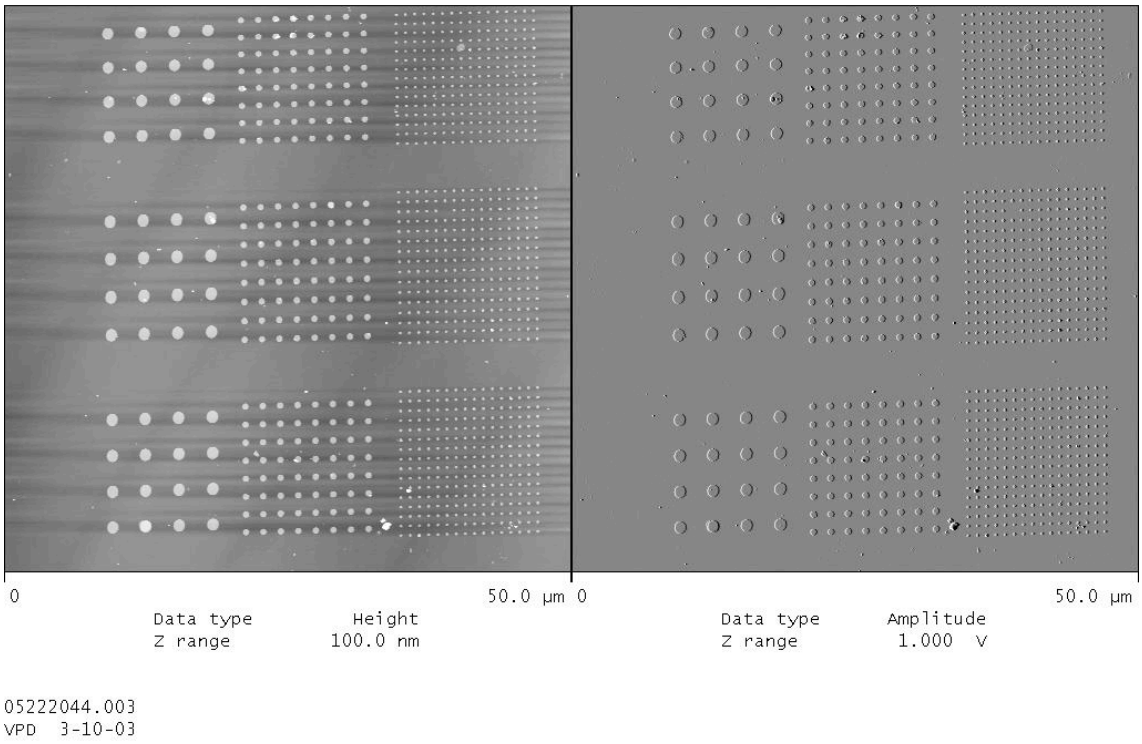

Figure 5.3: AFM of an array of dots patterned with the SEM and NPGS software. Left: Topographic image. Right: Tip ampltude image

deduced from a method involving FTIR spectroscopy, because it requires a surface area on the order of a millimeter in order to be effective. Another method of probing the electronic properties of a semiconductor on a nanometer scale must be explored.

5.2 Scanning Tunneling Spectroscopy

The scanning tunneling microscope (STM) has the ability to probe the surface density of states of a material used as a tunneling electrode, which earns the STM distinction as a tool of spectroscopy. The ability of the STM to be sensitive to the band structure of a material can be realized by an elementary knowledge of the theory of quantum mechanical tunneling.

Given a particle incident on a one-dimensional potential barrier, the Schrödinger equation is:

$$-\frac{\hbar^2}{2m}\frac{d^2}{dx^2}\psi + V(x)\psi = E\psi \tag{5.1}$$

where $\hbar$ is Panck's constant divided by 2π, m is the particle's mass, $V(x)$ is the potential of the barrier, E is the kinetic energy of the particle, and ψ is the wavefunction of the particle. Solutions of the Schrödinger equation are:

$$\psi(x) = \begin{cases} \mathrm{Ae}^{ikx} + \mathrm{Be}^{-ikx} & (\mathrm{x} < 0) \\ \mathrm{Ce}^{-i\kappa x} + \mathrm{De}^{i\kappa x} & (0 < \mathrm{x} < \mathrm{d}) \\ \mathrm{Fe}^{ikx} & (\mathrm{x} < \mathrm{d}) \end{cases} \tag{5.2}$$

where A, B, C, D,and F are amplitudes of the initial, barrier-reflected, in-barrier transmitted, within-barrier reflected, and out-of-barrier transmitted wavefunctions, respectively. The width of the barrier potential is d, $k = \sqrt{2mE}/\hbar$ is the magnitude of the particle's wavevector outside the barrier, and $\kappa = \sqrt{2m(V_\mathrm{o} - E)}/\hbar$ is the magnitude of the particle's wavevector inside the barrier. The probability of the particle transmitting through the potential barrier can be found to be:

$$T = \frac{FF^*}{AA^*} = \frac{16}{4 + (\frac{\kappa}{k})^2} e^{-2\kappa d} \tag{5.3}$$

assuming that $V(x)$ is much greater than E of the particle, and that the barrier width, d, is much larger than the wavefunction decay length, $1/k$. The transmission probability of a particle is exponentially dependent on barrier width, and this is the reason that the STM has the sensitivity to probe the surface density of states of a material. Practically, the measured tunneling current changes by orders of magnitude for Angstrom-sized differences in tip-sample separation [3,4].

Measurements of the density of states of a material provide the fundamental information necessary to calculate the direct band gap of a material. Also, the scanning tunneling microscope has the requirement that the sample areas being studied be less that 50 μm square, which makes STS an obvious tool for measuring the electronic properties of nanometer sized materials like those created with electron beam lithography. At present, efforts are focused on understanding the working mechanisms and eccentricities of the in-house STM. A mastering of the STS method of measuring electronic properties of semiconductors will surely open a new frontier in the characterization of EC-ALE films.

5.3 References

[1] *User's Manual for Nanometer Pattern Generation System v8 & v9, Instruction Manual* (J. C. Nabity LIthography Systems, Bozeman, MT, 2002).

[2] Web-site describing the Nanometer Pattern Generation System and related topics, http://www.jcnabity.com.

[3] J. A. Kubby and J. J. Boland, Surface Science Reports, **26**, (1996) 61.

[4] A. Beiser, *Concepts of Modern Physics, 5th ed.*, (McGraw-Hill, Inc., New York, 1995).